Peptide Amphiphile MRI Contrast Agent Relaxivity and Self-Assembly Behavior

Undergraduate Honors Research Thesis

Presented in Partial Fulfillment of the Requirements for graduation "with Honors Research Distinction in Chemistry" in the Arts and Sciences of The Ohio State University

By:

Aaron Andrew Manos

The Ohio State University

April 2016

Honors Defense Committee:

Professor Joshua Goldberger (Project Advisor)

Professor John Shimko

Professor Barbara Haeger

Table of Contents

Acknowledgements

Aaron would like to acknowledge the Goldberger Group, and specifically Christian Buettner, Dr. Arijit Ghosh, Mike Nicholl, and Ashley Wallace for their dedication and moral support of this project. Thanks to Dr. Elizabeth Hommel for training and support with the use of the Electrospray Ionization Mass Spectrometer. Thanks to Dr. Marina Bakhtina for training and support with the use of the Jasco Circular Dichroism Spectrometer. Thanks to Dr. Salim Ok for support with the minispec TD-NMR spectrometer. Thanks to The Ohio State University Department of Chemistry and Biochemistry for their continued commitment to providing the best undergraduate career in the nation.

Most importantly, thanks to Dr. Goldberger for the opportunity to research with the Goldberger Group, as well as unequaled help and guidance in your lab. I have learned so much through this experience, and I will certainly never forget it.

Vita

EDUCATION:

The Ohio State University, Columbus, OH

Bachelor of Science, Biochemistry, 2016

Minor in Creative Writing

Magna Cum Laude

Jackson High School, Massillon, OH

Honors Diploma, 2012

PUBLICATIONS:

A. Ghosh, C. J. Buettner, A. A. Manos, A. J. Wallace, M. F. Tweedle, J. E. Goldberger "Probing Peptide Self-Assembly in Serum" Biomacromolecules. 15 4488-4494, (2014).

Abstract

There has been an emerging interest in designing novel, biocompatible materials that can selectively undergo morphological transitions to accumulate at a cancer site in response to specific stimuli. One such stimulus is the acidic extracellular pH (6.6–7.0) of tumor tissue. Developing a magnetic resonance imaging (MRI) contrast agent that can self-assemble into a larger, more slowly diffusing entity only in the acidic extracellular pH would provide sufficient accumulation at the tumor site to allow it to selectively target all cancers and increase MRI resolution about the disease site. There is a significant challenge in achieving such a transition in vivo without understanding how the contrast agent structure can affect the self-assembly process. Here, we characterize the tunable self-assembling behavior of six peptide amphiphiles (PAs) from spherical micelles at higher pHs to cylindrical nanofibers at lower pHs. The molecular structure of each PA varies in the hydrophobic core, β-sheet forming, or charged region to assess how these changes affect self-assembly. The morphological pH and concentration dependence of the PAs was monitored in an isotonic salt solution mimicking that of blood serum using Critical Aggregation Concentration measurements and Circular Dichroism Spectroscopy. Moreover, the T_1 Relaxivity of the PAs was obtained to observe how morphological changes affect relaxation rates. It was found that increasing the length of the alkyl-tail, increasing the relative strength of the β-sheet forming region, and decreasing the relative strength of the charged region all function to increase the pH of transition, and vice-versa. These results provide a framework for optimizing PA structure to create a novel, pan-cancer, increased-resolution MRI contrast agent.

Chapter 1: Introduction

The American Cancer Society 1,700,000 new cases of cancer are expected to be diagnosed in the United States in 2016, and 13.0 million deaths are expected annually by 2030[1]. Accordingly, there has been a tremendous interest in developing new technologies to detect and treat cancer. Indeed, the National Institute of Health (NIH) estimates that 5.65 billion dollars will be spent in 2016 on cancer research[2]. A developing area of research is the use of specific biomarkers, such as hepsin in prostate cancer or CDX2 in colon cancer, as targets for drug delivery[3,4]. The World Health Organization (WHO) defines a biomarker as "any substance, structure, or process that can be measured in the body or its products and influence or predict the incidence of outcome or disease[5]."One such biomarker of cancer is the acidic extracellular environment surrounding the leaky vasculature of tumor tissue, caused by rapid growth and an increased rate of glycolysis[6,7]. This acidic environment of pH 6.6 – 7.2 is lower than that of normal physiological pH of 7.4. By exploiting these characteristics, a novel class of cancer-imaging materials can be developed. Specifically, a magnetic resonance imaging (MRI) contrast agent that can self-assemble into a larger, more slowly diffusing entity only in the acidic extracellular pH would provide sufficient accumulation to allow it to selectively target all cancers and increase MRI resolution about the disease site.

Peptide amphiphiles (PAs) are of interest due to their capacity to exist in a variety of morphologies, such as individual molecules, spherical micelles, or cylindrical nanofibers, depending on their concentration and environmental pH. We have previously demonstrated the ability of PAs to undergo a pH-triggered morphological transition *in vitro* from spherical micelle to cylindrical nanofiber in a serum that mimics that of tumor tissue[8]. This transition provides a diffusion-limited morphology that increases the local concentration of PAs at the disease site.

Figure 1 provides an overview of this mechanism. However, there is a significant challenge in achieving such a transition *in vivo* without understanding how the contrast agent structure can affect the self-assembly process, due to the various buffers and macromolecules present in organisms. To this end, we characterize the tunable self-assembling behavior of six peptide amphiphiles (PAs) from spherical micelles at higher pHs to cylindrical nanofibers at lower pHs. The molecular structure of each PA varies in the hydrophobic core, β-sheet forming, or charged region to assess how these changes affect self-assembly.

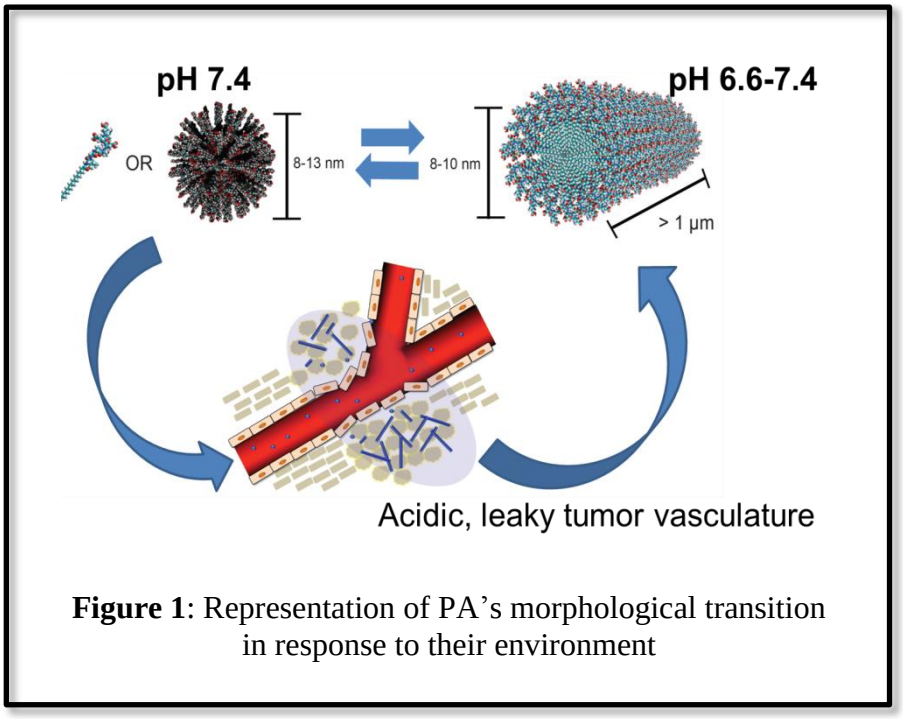

Figure 1: Representation of PA's morphological transition in response to their environment

The transition from micelle to nanofiber is necessary to take advantage of the enhanced permeability and retention (EPR) effect, which is a property of tumor tissue which allows the increased accumulation of small molecular aggregates due to the tissue's underdeveloped vascularization resulting from rapid tissue growth[9]. Micelles with diameters near 10 nm will be able to take advantage of the EPR effect, whereas their assembly into larger nanofibers with lengths in the micrometer range will be sterically hindered and unable to diffuse out of the

disease site. However, a molecule that can successfully transition *in vitro* may not necessary transition similarly *in vivo*. To this end, a more comprehensive understanding of how one can chemically tune the structure of PAs to affect their self-assembling function is necessary.

A typical PA consists of a hydrophobic alkyl tail and an amino acid sequence. Here, the amino acid sequence is composed of a more hydrophobic, β-sheet forming region, and a charged region of comparable size. We also attach a Gd^{3+} chelated 1,4,7-tris(carboxymethylaza)cyclododecane-10-azaacetylamide (DO3A) moiety to allow the molecules to be MRI active[10]. The length of the alkyl tail and the propensity of the β-sheet forming region to form β-sheet promotes the formation of nanofibers, whereas the relative strength of the charged region is primarily responsible for the formation of micelles under more basic conditions. All four aspects of the PAs (the alkyl tail, β-sheet forming region, charged region, and MRI region) affect the self-assembly process. A schematic representation of one of the PAs studied is provided in **Figure 2**.

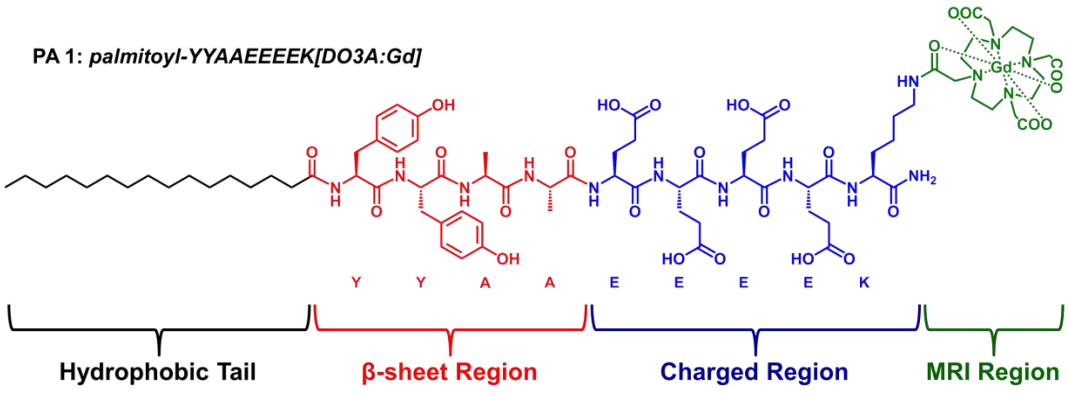

Figure 2: A colored representation of the structure of a peptide amphiphile

The attractive, nanofiber promoting forces and the repulsive, micelle promoting forces must be balanced in order to produce a molecule that can successfully transition *in vivo* at an acidic pH found within tumor tissues. To this end, we have previously synthesized and

characterized four PAs, varying the alkyl chain length, number of glutamic acids (E) in the charged region, and the substitution of tyrosine (Y) to alanine (A) in the β-sheet forming region. However, a more thorough understanding of how these structural changes affects transition required the characterization of two more PAs. The list of PAs synthesized and characterized are provided in **Table 1**. The scope of this project focuses on the synthesis and construction of phase diagrams of PAs 5 and 6, that is, pentadecyl-YAAAEEEEK(DO3A:Gd)-NH_2 and palmitoyl-YAAAEEEEEK(DO3A:Gd)-NH_2. Moreover, further characterization via T_1 relaxivity and dynamic light scattering (DLS) was acquired for PAs 1 – 6.

PA #	Structure
PA 1	palmitoyl-YYAA-EEEE-K[DO3A:Gd]
PA 2	palmitoyl-YYAA-***EEEEE***-K[DO3A:Gd]
PA 3	***pentadecyl***-YYAA-EEEE-K[DO3A:Gd]
PA 4	palmitoyl-***YA***AA-EEEE-K[DO3A:Gd]
PA 5	palmitoyl-***YA***AA-***EEEEE***-K[DO3A:Gd]
PA 6	***pentadecyl-YA***AA-EEEE-K[DO3A:Gd]

Table 1: PAs characterized.
Emphasis on how PAs 2 – 6 change from PA 1.

Chapter 2: Phase Diagrams of PAs 5 & 6

The PAs of this project were synthesized via solid-phase peptide synthesis using Fmoc chemistry and purified via preparatory scale reverse-phase high performance liquid chromatography (HPLC)[11]. Their purity was assayed via electrospray ionization time-of-flight mass spectrometry (ESI-TOF MS). The phase diagrams of PAs 1 – 4, including CD and CAC measurements, were previously determined by Nicholl[12]. Accordingly, this project aims to further elucidate structure-function relationships via determination of the phase diagrams of PAs 5 & 6. As discussed by Nicholl, palmitoyl-YYAAEEEEK(DO3A:Gd)-NH_2 (PA 1) exclusively formed nanofibers over micelles or individual molecules across all pHs and concentrations examined, due to the molecule's dual tyrosine (Y) residues which exhibit a high β-sheet forming propensity[13]. Therefore, the goal of characterizing PAs 2 – 6 was to decrease the attractive forces. This was accomplished by adding an additional glutamic acid (E) to the charged region for PA 5, and removing a methylene group in the hydrophobic region for PA 6. For all measurements, PAs were dissolved in a 150 mM NaCl, 2.2 mM $CaCl_2$ simulated serum salt solution to replicate the electrostatic environment found in animal plasmas.

Because the PAs studied can exist as three different morphologies, a combination of Circular Dichroism (CD) and Critical Aggregation Concentration (CAC) were used to construct phase diagrams illustrating the pH and concentration dependence of the PAs. CD was used to gauge the morphology transition between spherical micelles and cylindrical nanofibers. On the CD graph, the micelle morphology is specified by the characteristic "random coil" spectrum, indicated by a relatively mild local maximum around 218 nm. The nanofiber morphology is specified by the characteristic "β-sheet" spectrum, indicated by a more intense local minimum

around 218 nm. Because the transition between the two morphologies is not dichotomous and exact, the working definition of a transition as detected by CD is when the first β-sheet spectrum crosses the x-axis at 205 nm, which was previously confirmed by fluorescence anisotropy[14]. CAC was used to gauge the concentration at which PA aggregated from individual molecules into either micelles or nanofibers using the pyrene 1:3 method[15]. On the CAC graph, the CAC is determined where there is a change in slope of the ratio of the first and third (I_{376}/I_{392}) emissions of pyrene when excited at 335nm. The change in slope of I_{376}/I_{392} is the result of the encapsulation of pyrene into the micelles or nanofibers at higher concentrations. The phase diagrams of PAs 5 & 6 are provided in **Figure 3**.

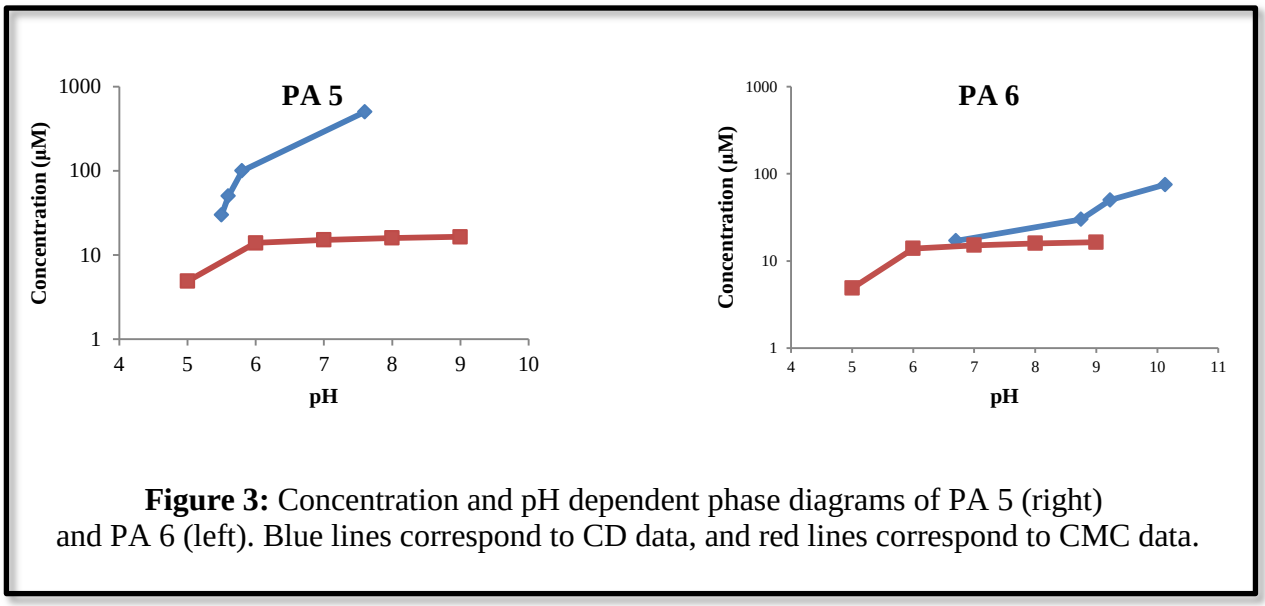

Figure 3: Concentration and pH dependent phase diagrams of PA 5 (right) and PA 6 (left). Blue lines correspond to CD data, and red lines correspond to CMC data.

Chapter 3: Comparison of Phase Diagrams

I) Circular Dichroism

The transition from spherical micelles at more basic pHs to cylindrical nanofibers at more acidic pHs is crucial to the development of this class of imaging-vehicle delivery. For PA 1, there was no observable transition from CD across a wide range of pH values and concentrations. However, micelle to nanofiber pH dependent transitions did occur in PAs 2 – 5. A comparison of this CD transitional pHs for the five molecules is provided in **Figure 4.**

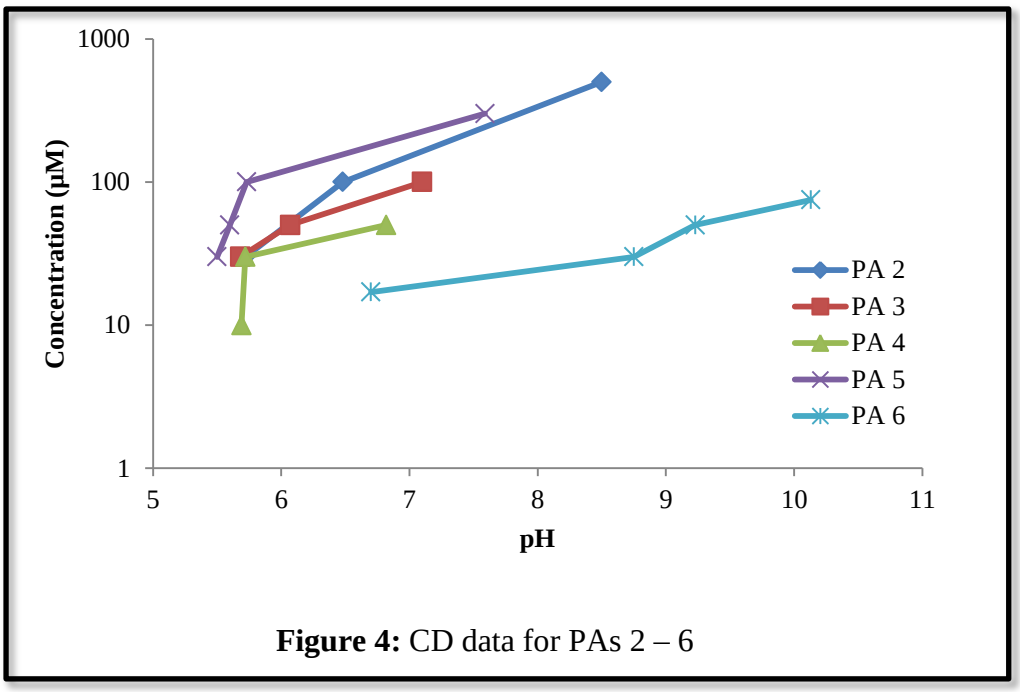

Figure 4: CD data for PAs 2 – 6

From this data, we can see that there is a concentration dependence on their pH of transition, especially at more basic pHs, most notably in PA 6. This concentration dependence has been noted in the past, albeit to a lesser extent, which is not desirable in a delivery vehicle. Other PAs, such as palmitoyl-IAAAEEEEK(DOTA:Gd) and palmitoyl-MAAAEEEEK(DOTA:Gd), are better suited for this contrast imaging delivery method due to

their relative concentration independence. Therefore, this concentration dependence may be due to the presence of the amphipathic tyrosine residues in the β-sheet forming region. Tyrosine's side group both contains an aromatic ring and a hydroxyl group, which could influence self-assembly due to pi-pi interactions and hydrogen bonding interactions, respectively.

Because comparisons between PAs 2 – 4 are provided by Nicholl, this discussion will focus on comparisons between PA 5 with PAs 2 – 4, PA 6 with PAs 2 – 4, and PA 5 with PA 6. Out of the YAAA PAs (PAs 4 – 6), PA 5 containing an extra glutamic acid, has the most acidic pH of transition. Coupled with the fact that out of the YYAA PAs (PAs 1 – 3), PA 2 containing an extra glutamic acid, has the most acidic pH of transition, we can see that adding a glutamic acid lowers the pH of transition, and therefore serves as a repulsive force to form micelles over nanofibers.

Interestingly, PA 6's CD shows that out of the YAAA PAs (PAs 4 – 6), it has the strongest preference to form nanofibers over micelles. There is evidence that the deletion of a methylene group is certainly a repulsive force because PA 1 contained the longer palmitoyl alkyl chain and was always nanofibers, whereas PAs 3 and 6 contained the shorter pentadecyl alkyl chain and both exhibited transitions into micelles at some pH. Therefore, for YAAA PAs, the addition of an extra glutamic acid has greater influence on the nanofiber forming ability of the PA than the deletion of a methylene group. The most confounding data in this study is the fact that PA 6 appears to form nanofibers more preferentially than PA 4, which has the same amino acid sequence but the palmitoyl alkyl chain. It may also be the case that the relative inability of the pentadecyl alkyl chain to undergo a hydrophobic collapse disproportionately alters the desolvation cost of the β-sheet forming region to prefer a β-sheet configuration, which is not seen in PA 3 due to the presence of the second tyrosine, which is better solvated by water due to

the free hydroxyl group on the side chain. Admittedly, the difficulty of trying to explain this phenomenon is not lost, and a more likely candidate is simply that the data points from the PA 6 CD are errant. Ideally, the CD curve on the phase diagram would be above PA 4 and below PA 6, which would indicate a proper loss of attractive forces by the presence of the pentadecyl and β-sheet amino acid subsitutions.

II) Critical Aggregation Concentrations

By using CAC, we can determine the propensity for PAs to form micelles or nanofibers versus individual molecules. These measurements provide information regarding the minimum concentration needed to inject into a test subject to achieve enhanced resolution via MRI. Ideally, PAs would exist in the micelle morphology at the physiological pH of 7.4. **Figure 5** shows a comparison of CAC measurements for PAs 2 – 5, as the CAC of PA 1 was below the detectable limit.

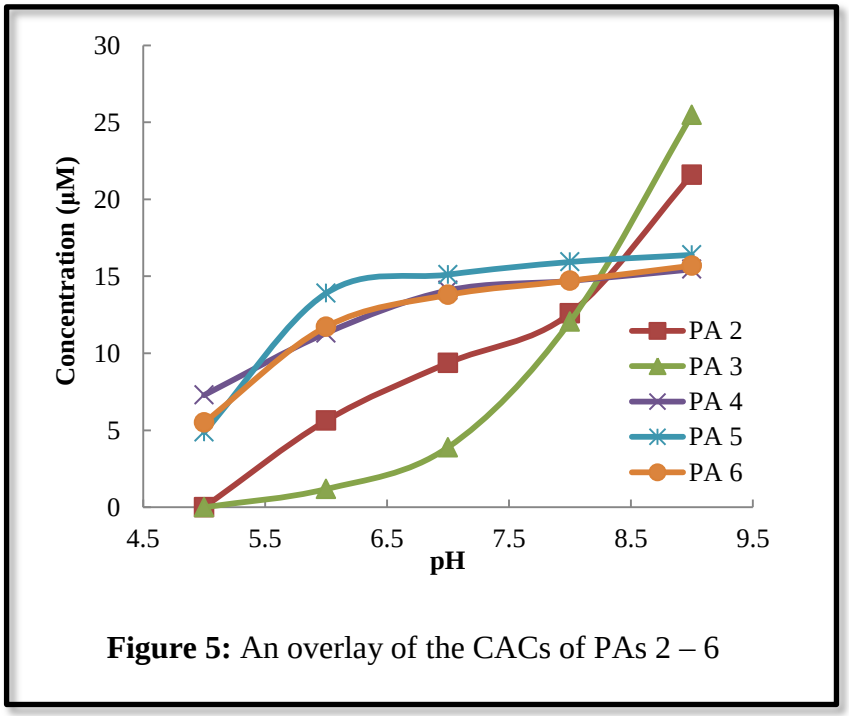

Figure 5: An overlay of the CACs of PAs 2 – 6

Foremost, this data shows that PAs 2 – 5 do aggregate from individual molecules into nanofibers or micelles at pH 5 – 9. This is evidence of reduced attractive forces due to the structural changes imposed. PAs 2 & 3 have two tyrosines in their β-sheet forming regions, as opposed to the singular tyrosine in PAs 4 – 6. The increased hydrophobic interactions caused by the extra tyrosine allow PAs 2 & 3 to self –assemble easier. Accordingly, at pH 5 – 8, the CAC of PAs 2 & 3 are both lower than those of PAs 4 – 6. However, at pH 9, PA 3 has the highest CAC, followed by PA 2. At this pH, the glutamic acids in the charged region will be largely deprotonated and exhibit a negative charge, which can serve as a repulsive force. Interestingly, we do not see this behavior in PAs 4 – 6. Therefore, there is evidence that this CAC discrepancy is caused by the deprotonation of the two tyrosines due to the approach of the pH to its pKa of 10.07.

We can also see that the CAC for all PAs is lowest at pH 5. Moreover, for PAs 4, 5, and 6, there is a relatively large jump between the CACs of pH 5 and 6. This may be due to the morphology that the individual molecules are aggregating into. At low concentrations, the pH of transition for most PAs is near 5.5. This is most directly illustrated by PAs 4 and 5. Therefore, it may be the case that the PAs are assembling into nanofibers in the pH range 5 – 6 and have a stronger propensity to form nanofibers than micelles at this pH.

We can see that the deletion of a methylene group has less influence over the CAC than adding a glutamic acid. For instance, the CAC of PA 1 was below the detectable limit, and at pHs 5 – 8, PA 3 also had the lowest CACs for PAs 2 – 6. Similarly, PA 6 had a slightly higher CAC than PA 4 at pH 6 – 9, indicating that the deletion of the methylene was indeed a repulsive force for the transition between individual molecules and an aggregate, but less so than adding a glutamic acid.

Interestingly, whereas PA 6 preferentially formed nanofibers more than any PA other than PA 1, it did not have the lowest CAC. This indicates that PA 6 prefers to exist as a single molecule or nanofiber over a micelle, relative to the rest of the PAs. The explanation for this phenomenon remains to be seen.

III) Phase Diagrams

The ability for our PAs to exist as single molecules, micelles, and nanofibers adds complexity to their analysis. The molecules preference for single molecules over micelles does not necessarily have much bearing on their preference to form micelles over nanofibers. However, by overlaying the phase diagrams, we can analyze the PAs preference to form each morphology as a function of their chemical structure. One of the limitations of this analysis is that PA 1 only formed nanofibers, and accordingly cannot be used to compare how its self-assembly compares to those of other molecules. Nevertheless, comparisons can be made to assess how each of the structural changes – adding a glutamic acid, removing a methylene group, substituting a tyrosine for an alanine – affected self-assembly.

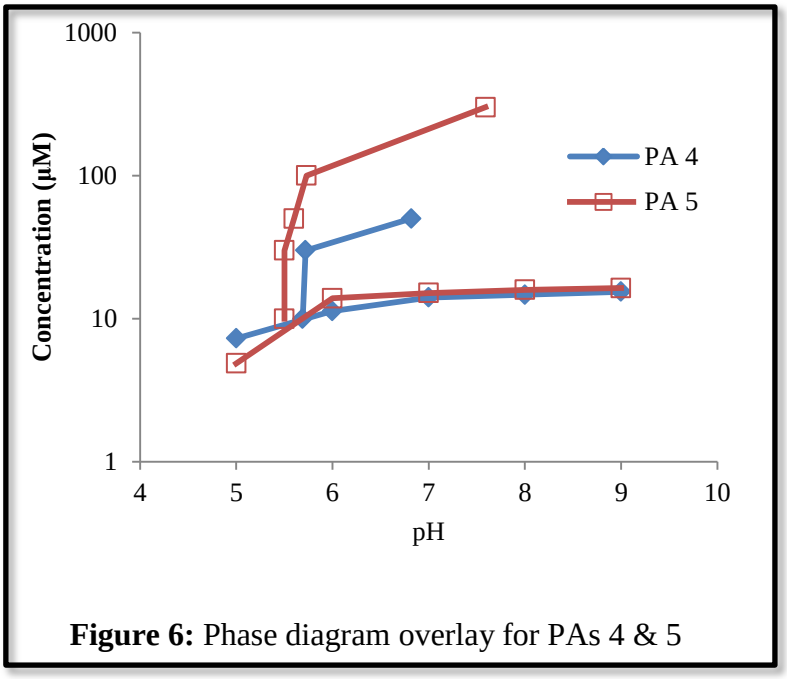

Figure 6: Phase diagram overlay for PAs 4 & 5

Figure 6 shows the comparison between PAs 4 & 5, with the structural change being adding a glutamic acid in the charged region. Going from PA 4 to PA 5, the region where micelles can exist expands, indicating that adding an additional glutamic acid reduces the attractive forces. Similarly, for pHs 6 – 9, the CAC of PA 5 is higher than that for PA 4. At pH 5, we can see that the CAC for PA 5 is lower than that of PA 4, which indicates that PA 5 will form a nanofiber more readily than PA 4. Thus, the addition of a glutamic acid may be seen as an attractive force only at low concentrations and pHs, which may be due to the differences in pKas of the carboxylic acids of the glutamic acids, which are influenced by their local environment. For instance, the pKa of acetic acid, a common monoprotic carboxylic acid, is 4.76 at 25 ºC. However, the pKas of malonic acid, a dicarboxylic acid with a methylene group between the carbonyls, are 2.85 and 5.70 at 25 ºC[16]. The glutamic acids in close proximity to each other makes it more challenging to remove subsequent protons to introduce new negative, repulsive charges, which in turn, allows the additional glutamic acid to function as an attractive force at this acidic pH.

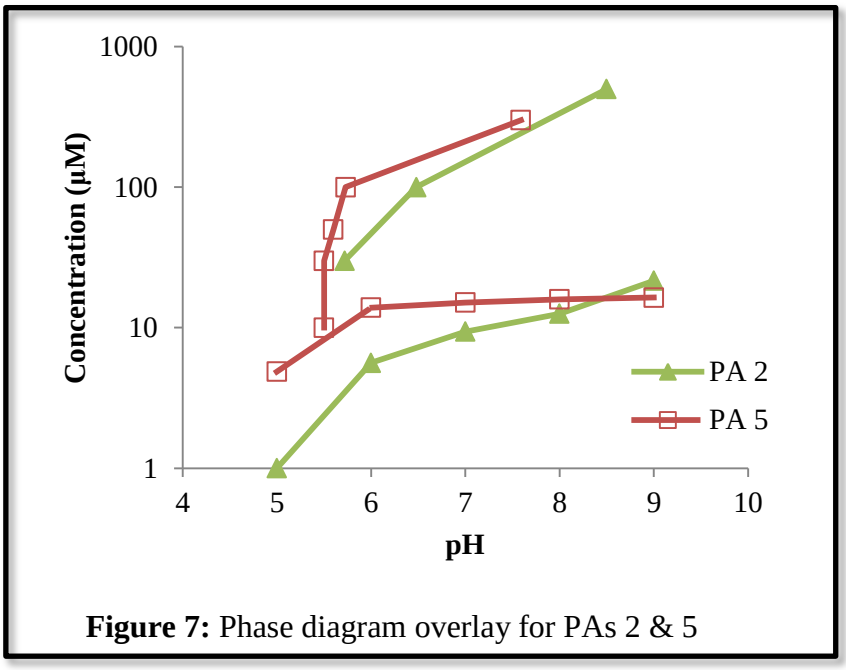

Figure 7: Phase diagram overlay for PAs 2 & 5

Figure 7 shows the comparison between PAs 2 & 5, with the structural change being the substitution of a tyrosine for an alanine in PA 5. As with the previous comparison, the area for micelle region transforms. The CD curve shifts to the left, indicative of the loss of attractive forces offered by the second tyrosine in the β-sheet forming region. Similarly, across pHs 5 – 8, the CMC increases, indicative of a loss of attractive forces. As discussed previously, at the high CMC value at pH 9 for PA 5 may be due to the deprotonation of the tyrosines. In a similar manner to how the polarizable carboxylic acids' pKas changed due to their environment, the tyrosines in close proximity to each other induce a gap between their two pKas – for instance, from the literature value of 10.07 for each tyrosine, to approximately 9 and 11.

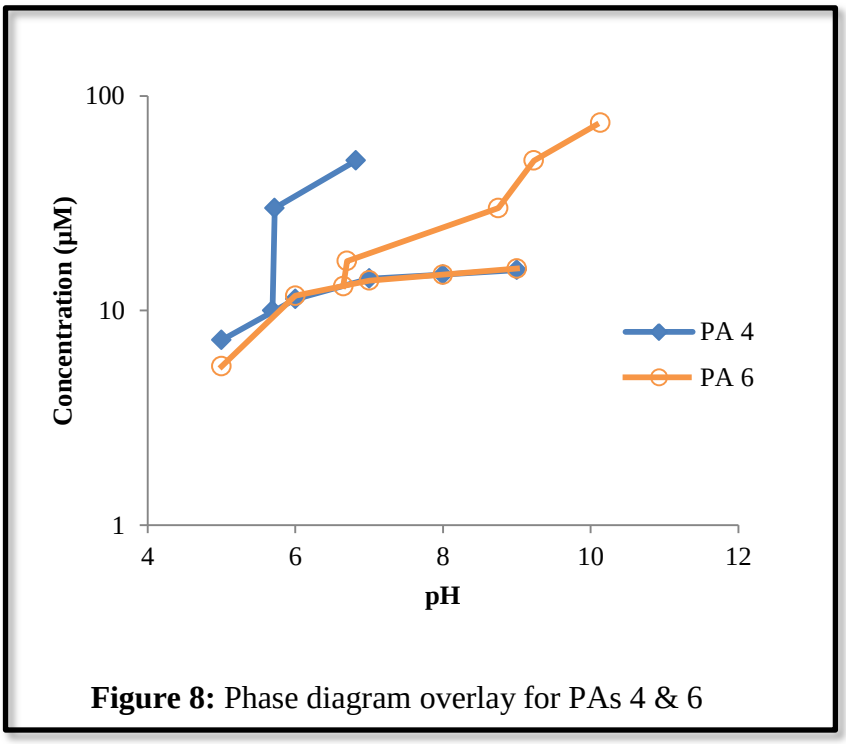

Figure 8: Phase diagram overlay for PAs 4 & 6

Figure 8 shows the comparison between PAs 4 & 6, with the structural change being the removal of a methylene group in the alkyl chain in PA 6. The CMCs are very similar, although at all pHs except for pH 5, PA 6 has a slightly smaller CMC. The decreased region where micelles

can form is unexpected, and in light of any better explanation, the CD data may have been incorrectly determined. The most likely candidate for error was an increased concentration of stock solution. Materials containing tyrosine absorb very well in the 275 to 280 nm range due to the aromatic groups on the side chains[17]. Therefore, some of this absorbance might be able to be detected at the high end of the CD absorbance, which was determined for wavelengths 190 – 260 nm. Unfortunately, there was no indication of bleed-over in the 255 – 260 nm wavelengths for the CD of PA 6, so this concentration determination method cannot be used.

Chapter 4: Dynamic Light Scattering

Dynamic Light Scattering (DLS) was employed to analyze the size of micelles. DLS uses the random movement, i.e., Brownian motion, of smaller particles that are faster than the movement of larger particles to determine the size of spherical particles. Fluctuations in the intensities of light scattered by the particles can be determined and the translational diffusion coefficient derived. Using the Stokes-Einstein equation, the hydrodynamic radius can be calculated.

The average diameters of micelle-forming PAs 2 – 6 are summarized in **Figure 9**. The ± values represent one weighted standard deviation for the error associated with collecting these data, and not one standard deviation of the actual size of the micelles. This is to say, for PA 2, the micelle most likely has a diameter of 11.26 nm, but it may be slightly bigger or smaller. The ± values should not be interpreted as the micelles size existing on a continuum, with some being smaller than the average and some being larger. Accordingly, it may seem promising that PAs 3 & 6 are smaller than PAs 1 & 4 (pentadecyl to palmitoyl, respectively), this cannot be seen as statistically significant. However, while this data is not exact, it provides a foundation for further analysis, and with a lack of other evidence present, provides information on the sizes of the micelles.

Diameter (nm)	
PA 2	***11.26 ± 1.53***
PA 3	***10.81 ± 1.56***
PA 4	***10.97 ± 1.85***
PA 5	***11.21 ± 1.77***
PA 6	***10.75 ± 1.45***

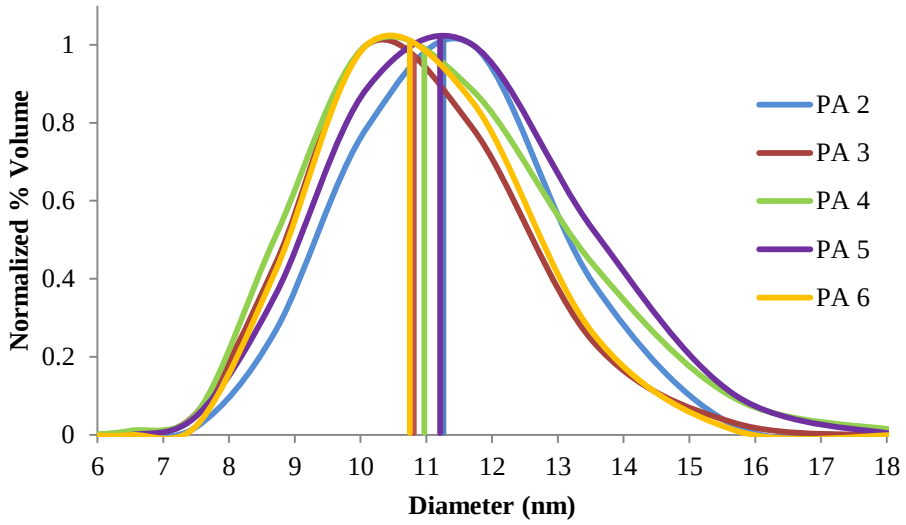

Figure 9: The weighted average diameters and normalized DLS curves

Interestingly, the weighted average diameters of PAs 2 and 5 are approximately 0.3 – 0.4 nm larger than those of PAs 3, 4, and 6. This is indicative of the presence of one additional glutamic acid in the charged region, as that length roughly corresponds to roughly less than the size of two additional amino acids, due to the diameter being composed of two PAs. Similarly, the weighted average diameters of PAs 3 and 6 are smaller than that of PA 4, indicative of a loss of a methylene group in the hydrophobic core.

Chapter 5: T_1 Relaxivity (r_1)

A critical component of this study is to study how well the different morphologies function as MRI contrast agents. In order to assess this, low-field spin−lattice (T_1) values of PAs 1 – 6 were determined in 150 mM NaCl and 2.2 $CaCl_2$ mM aqueous solution. Three regions of each PA's phase diagram were studied: the nanofibrous range below the concentration-independent pH of transition, the high concentration nanofibrous range above the pH of transition, and the micellar range above the pH of transition concentration-independent, as demonstrated in **Figure 10**. This would require a systematic determination of T_1 values at a minimum of two pHs: a more acidic pH and a more physiologically relevant pH. At very acidic pHs < 5.0, DO3A is known to leech Gd^{3+} due to the protonation of the carboxylic acids chelating the metal ligand (biomac?). Bound Gd is necessary for inner-sphere paramagnetic relaxation about the DO3A complex, and aqueous Gd^{3+} is toxic to mammals[18]. Therefore, a pH of 5.2 was selected to ensure Gd^{3+} remained chelated, and because all PAs exist as nanofibers at this pH above their CACs. As noted earlier, tumors tissues are more acidic than normal tissues. For this reason, a pH of 7.0 was selected to assess how the concentration-dependent transition from nanofiber to micelle affected relaxation times. T_1 relaxivity (r_1) was determined according to the equation

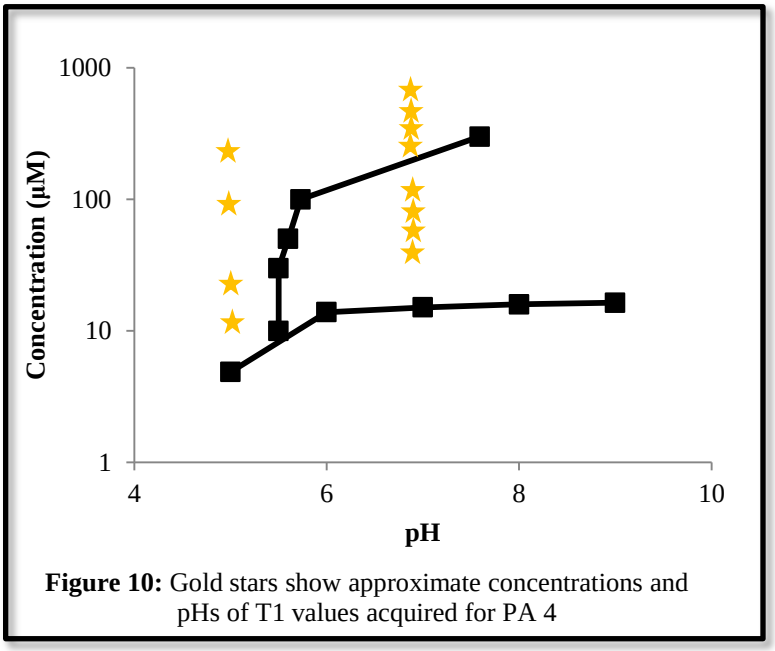

Figure 10: Gold stars show approximate concentrations and pHs of T1 values acquired for PA 4

$$1/T_1 = 1/T_{1,d} + r_1[\text{contrast agent}]$$

where $1/T_{1,d}$ corresponds to salt solution proton relaxation time in the absence of the paramagnetic contrast agent, PA(DO3A:Gd).

The r_1 values for PAs 1 – 6 are provided in **Table 2**. Here, we can see that the relaxivity of nanofibers at pH 5.2 and 7.0 are all within 10% of each other, indicating that they exhibit similar relaxation activities. Moreover, we can see that all nanofibrous relaxivities are significantly higher than their micellar counterparts. This is due to an increased rotational correlation time of the PA(DO3A:Gd) with the water lattice as a result of the higher molecular weight and slower tumbling time of the nanofiber morphology.

PA #	pH 5.2 Nanofiber r_1	pH 7.0 Nanofiber r_1	pH 7.0 Micelle r_1
PA 1	10.51	10.58	-
PA 2	10.24	9.95	4.89
PA 3	9.51	8.49	5.09
PA 4	10.19	9.33	7.65
PA 5	8.53	8.54	5.69
PA 6	9.60	9.09	6.47

Table 2: r_1 values for the PAs

Similarly, we see that, although E_5 PAs 2 & 5 have larger molecular weights and increased diameters as compared to their E_4 PAs 1 &4 counterparts, they have lower r_1 values. This may be due to additional degrees of freedom offered by the additional charged amino acid in the charged region. These results are promising because they show that PA(DO3A:Gd) exhibit increased relaxivity compared to an FDA-approved Prohance/Gadoteridol control (r_1 = 4.1 L $mmol^{-1}$ s^{-1})[14].

Chapter 6: Conclusions and Future Work

In conclusion, we have shown the ability to tune the self-assembly behavior of PAs in an isotonic salt solution by chemically modifying the hydrophobic tail, β-sheet forming, and charged regions. Since PA 1 was seen to have too great attractive forces which induced a morphology of nanofibers at all concentrations and pHs, the following effects were found to decrease these repulsive forces to induce micelle formation: shortening the hydrophobic tail (palmitoyl to pentadecyl), substituting amino acids in the β-sheet forming region for amino acids that have a lesser propensity to form β-sheets (YYAA to YAAA), and adding an additional charged amino acid in the charged region (EEEE to EEEEE). An immediate need of this project is to acquire cryo-TEM images of PAs 5 & 6 to better visualize the morphologies of the molecules. Similarly, we may desire to recollect the CD data for PA 6.

It is worth noting that PAs 1 – 6 would not make for ideal transitioning vehicles *in vivo*. Foremost, their pHs of transition on the whole are too low in comparison to an ideal transitioning pH near 6.8 – 7.0. However, the primary reason to not use these tyrosine-containing PAs is their remarkable concentration dependence, as seen by the higher horizontal lines in the phase diagrams. A more ideal PA's self-assembly would be concentration independent, that is, the PA will always transition from micelle to nanofiber at a specific pH regardless of the concentration. For instance, recent unpublished murine *in vivo* experiments require the injection concentration of PA to be >1mM – because the animals are only 20-25g – at which PAs 1 – 6 would firmly be nanofibers. While the PAs will dilute to roughly 50 μM by the time they reach the tumor site, injecting micelles would be kinetically simpler. Nevertheless, a complete biodistribution study

with PA-DO3A:Gd will be necessary to more fully understand the future direction of this project.

We have found that a similar palmitoyl-MAAAEEEEK(DO3A:Gd) system is too small and overwhelmingly accumulates in the kidneys and organs with strong immune system activity, such as the lungs, spleen, and liver. This is indicative a small hydrodynamic radius and uptake by the mononuclear phagocyte system (MPS). To counteract these conditions, addition of polyethylene glycol (PEG) could be used. PEG is a ubiquitous, FDA-approved polymer used to coat biomaterials such as proteins, micelles, liposomes. Adding PEG will require additional considerations as to how adding a bulky hydrophilic, polydisperse group to the periphery of the PA affects self-assembly. Moreover, chain length and graft density – the percent of molecules within a micelle that contain the PEG – will further complicate this analysis. Regardless, PEGylation will be a vital component in the development of this next-generation contrast agent.

Chapter 7: Supporting Information

Mass Spectrometry

PA 5: palmitoyl-YAAAEEEEEK(DO3A:Gd)-NH_2 (Exact Mass: 1945.82 g/mol)

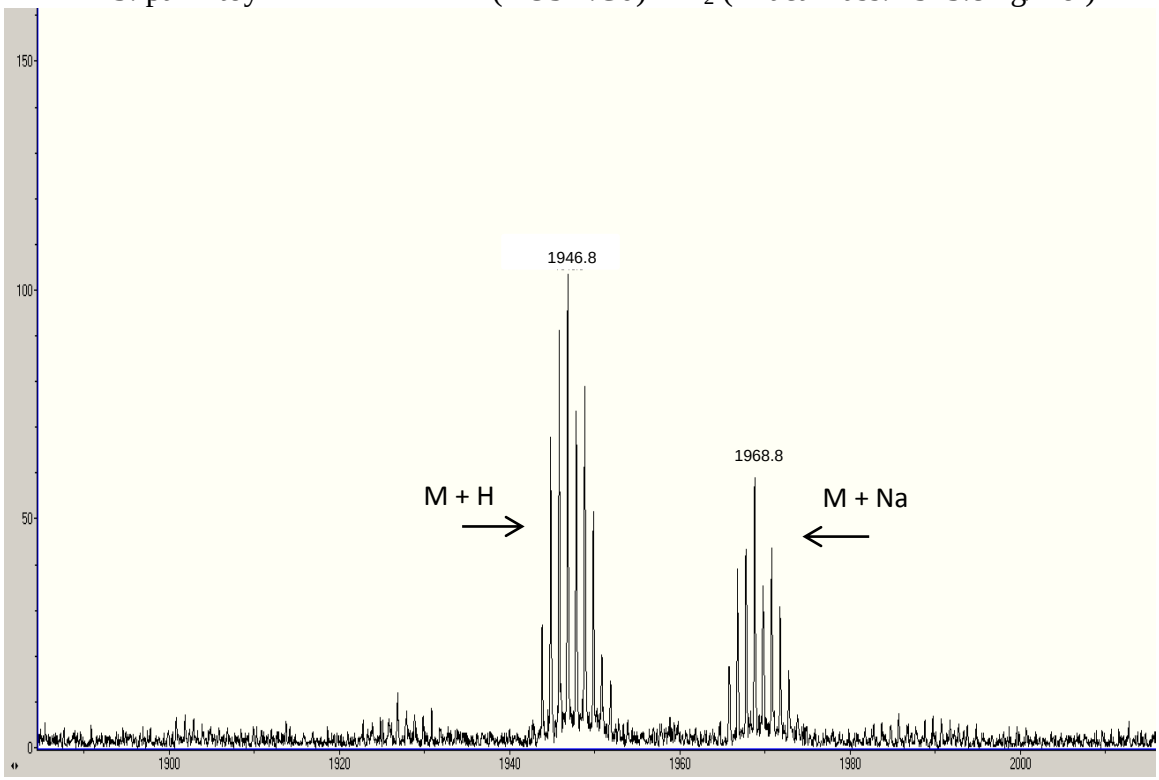

PA 6: pentadecyl-YAAAEEEEK(DO3A:Gd)-NH_2 (Exact Mass: 1802.76 g/mol)

1825.7

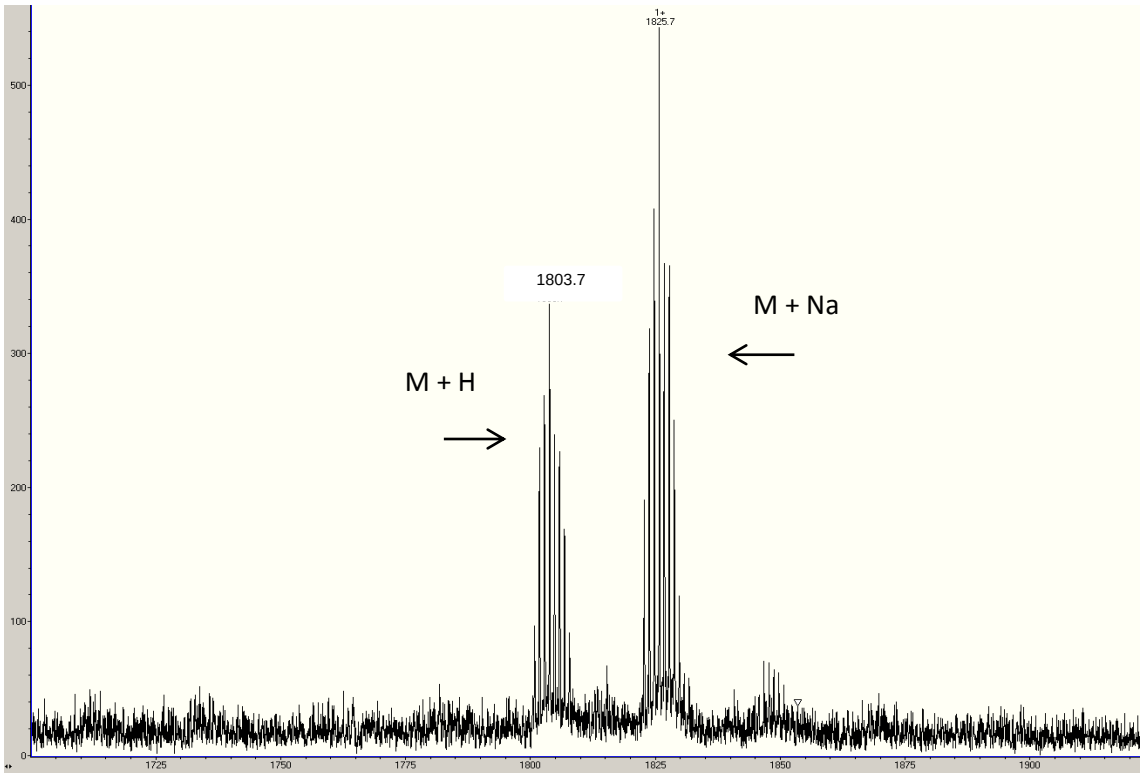

Circular Dichroism

CD PA 5 at different concentrations in 150 mM NaCl and 2.2 mM $CaCl_2$

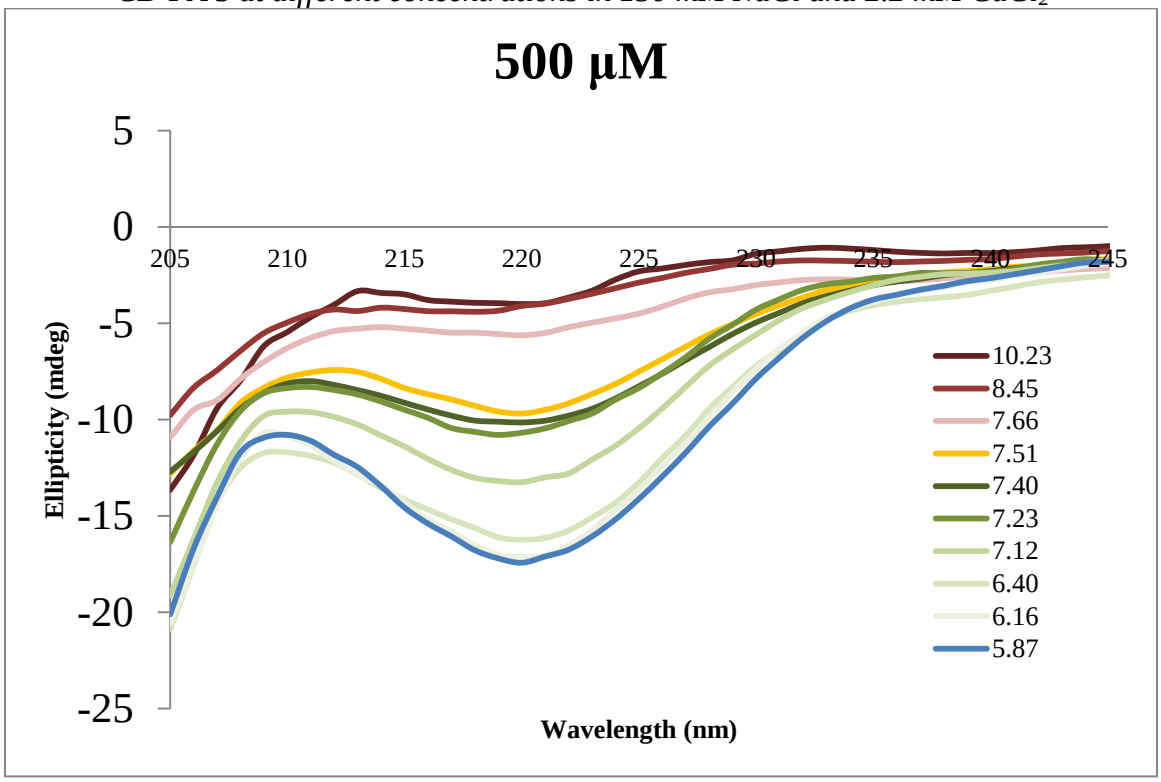

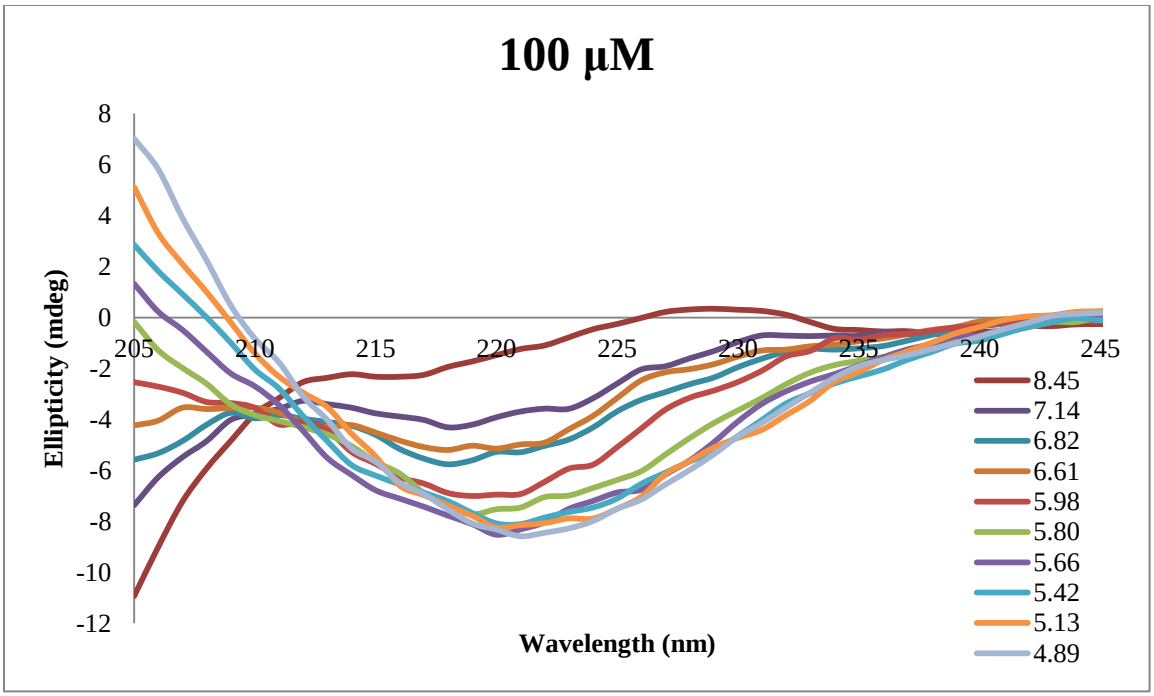
100 µM
Ellipticity (mdeg)
8
6
4
2
0
-2
-4
-6
-8
-10
-12
205
210
215
220
225
230
235
240
245
Wavelength (nm)
8.45
7.14
6.82
6.61
5.98
5.80
5.66
5.42
5.13
4.89

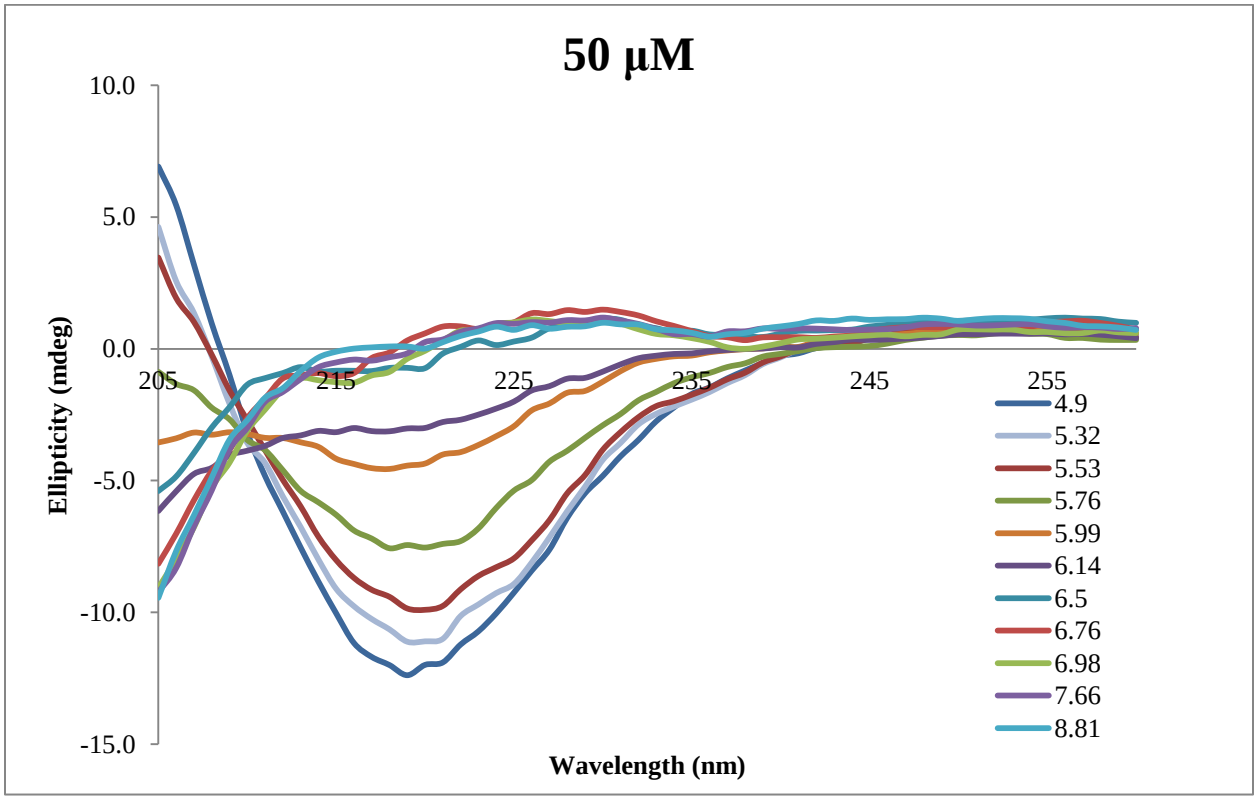
50 µM
Ellipticity (mdeg)
10.0
5.0
0.0
-5.0
-10.0
-15.0
205
215
225
235
245
255
Wavelength (nm)
4.9
5.32
5.53
5.76
5.99
6.14
6.5
6.76
6.98
7.66
8.81

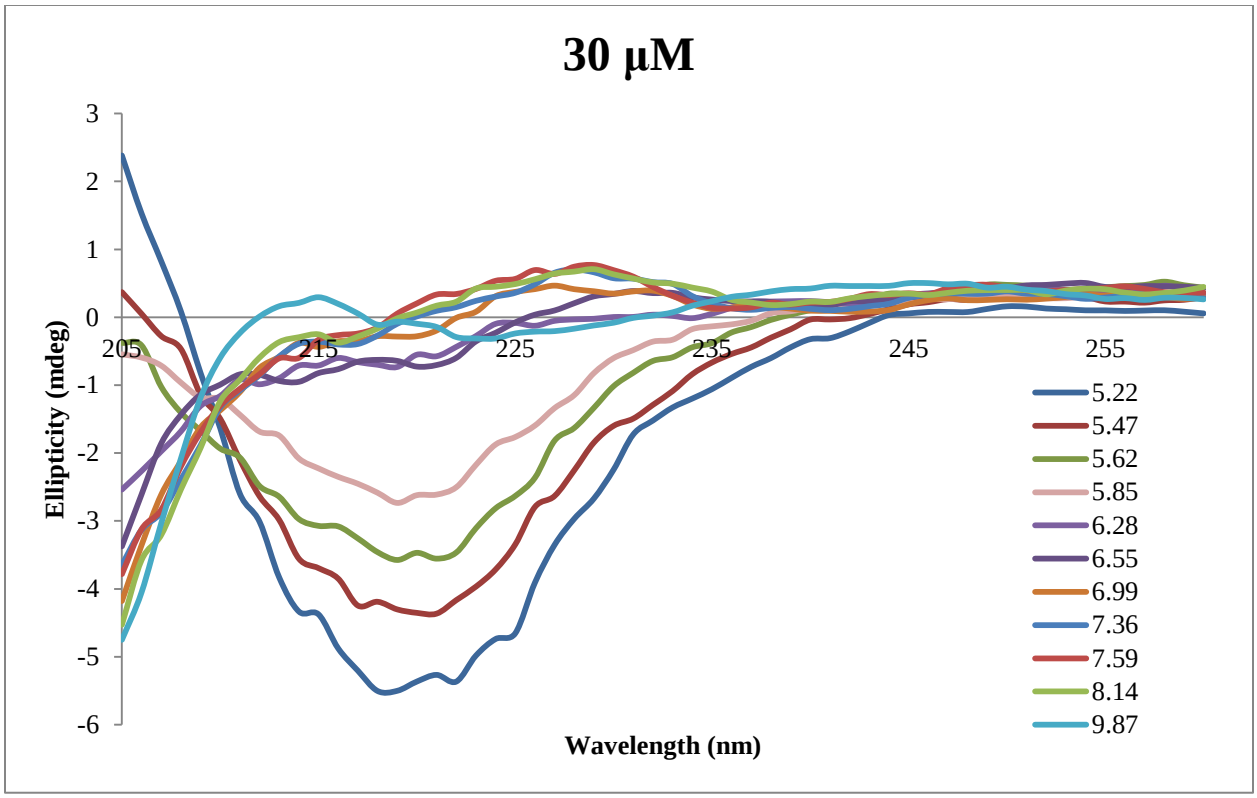

CD PA 6 at different concentrations in 150 mM NaCl and 2.2 mM $CaCl_2$

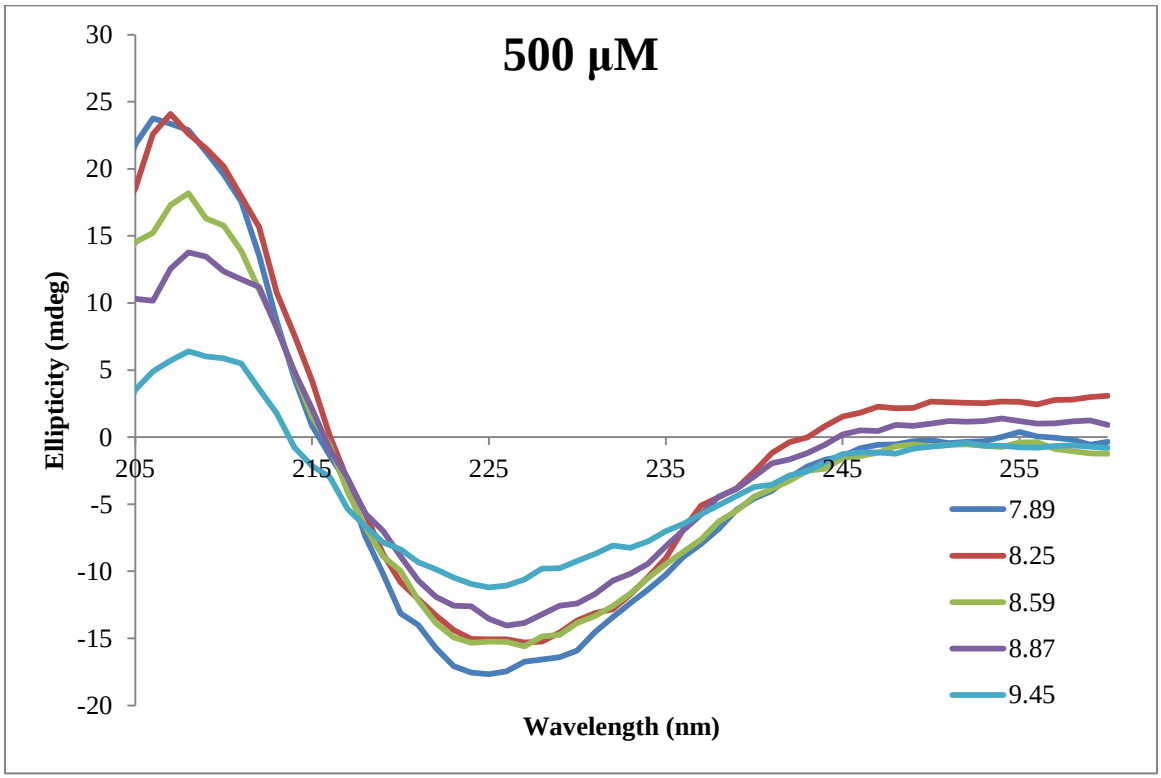

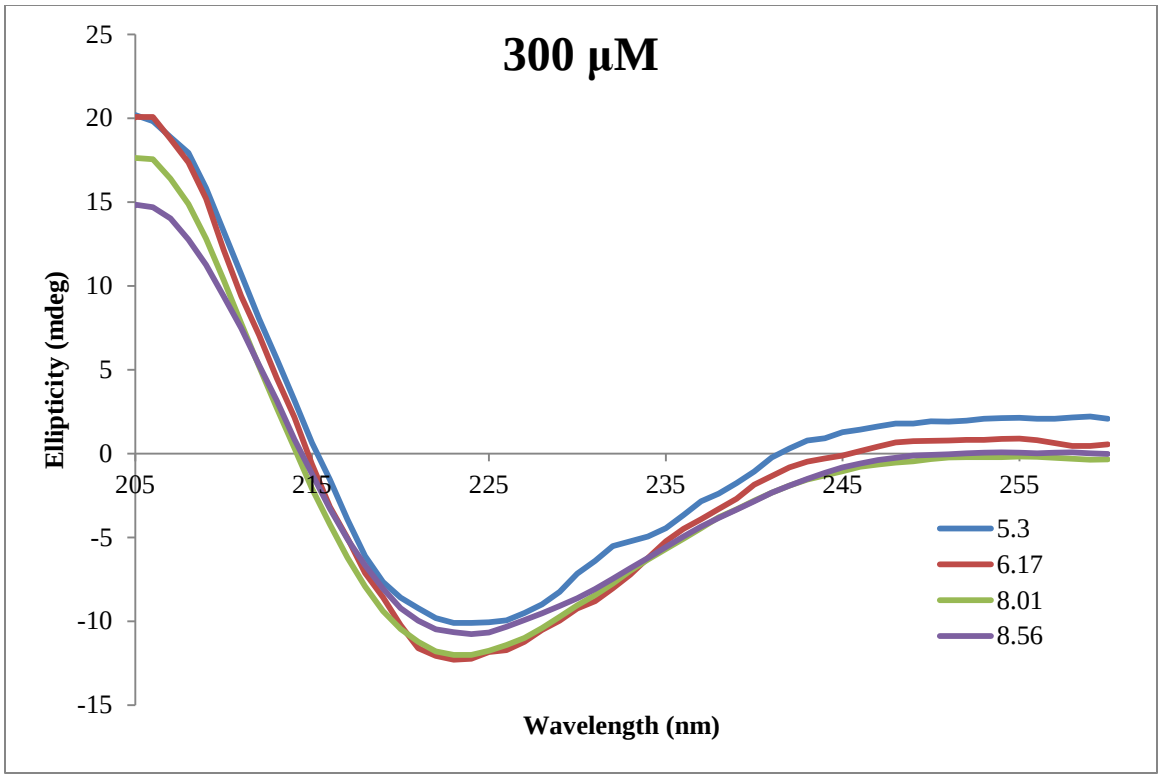
300 µM
Ellipticity (mdeg)
25
20
15
10
5
0
-5
-10
-15
205
215
225
235
245
255
Wavelength (nm)
5.3
6.17
8.01
8.56

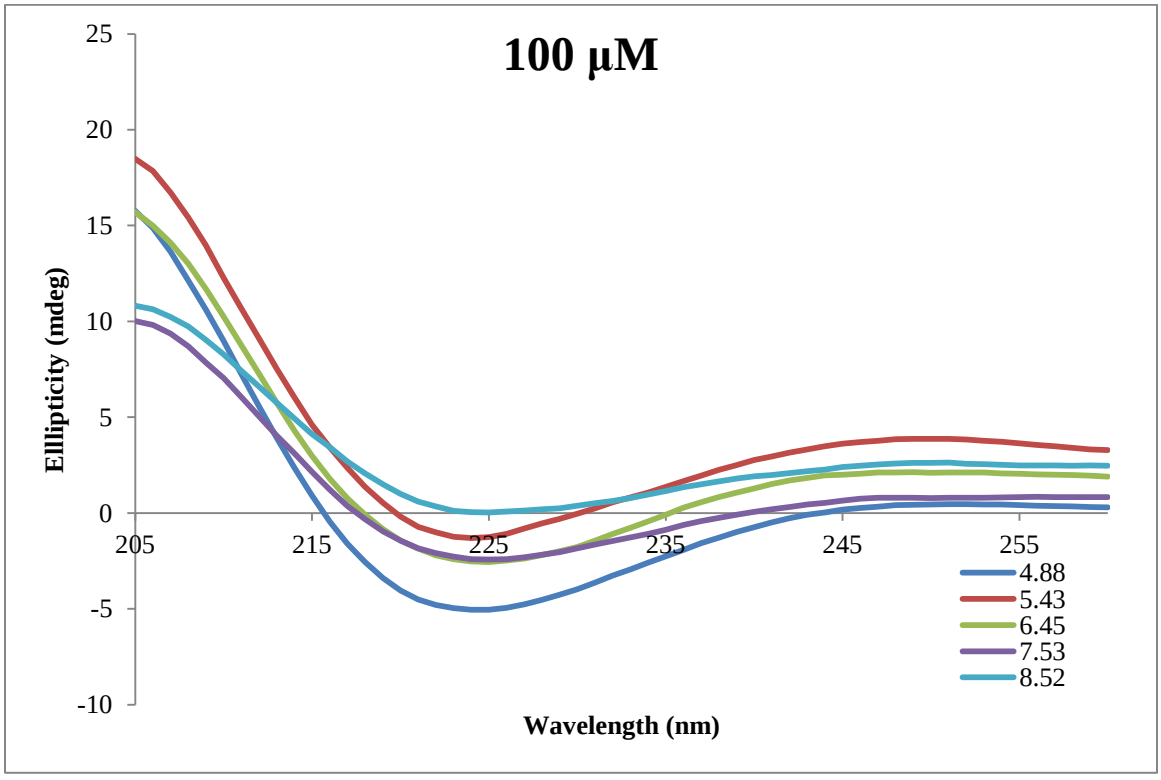
100 µM
Ellipticity (mdeg)
25
20
15
10
5
0
-5
-10
205
215
225
235
245
255
Wavelength (nm)
4.88
5.43
6.45
7.53
8.52

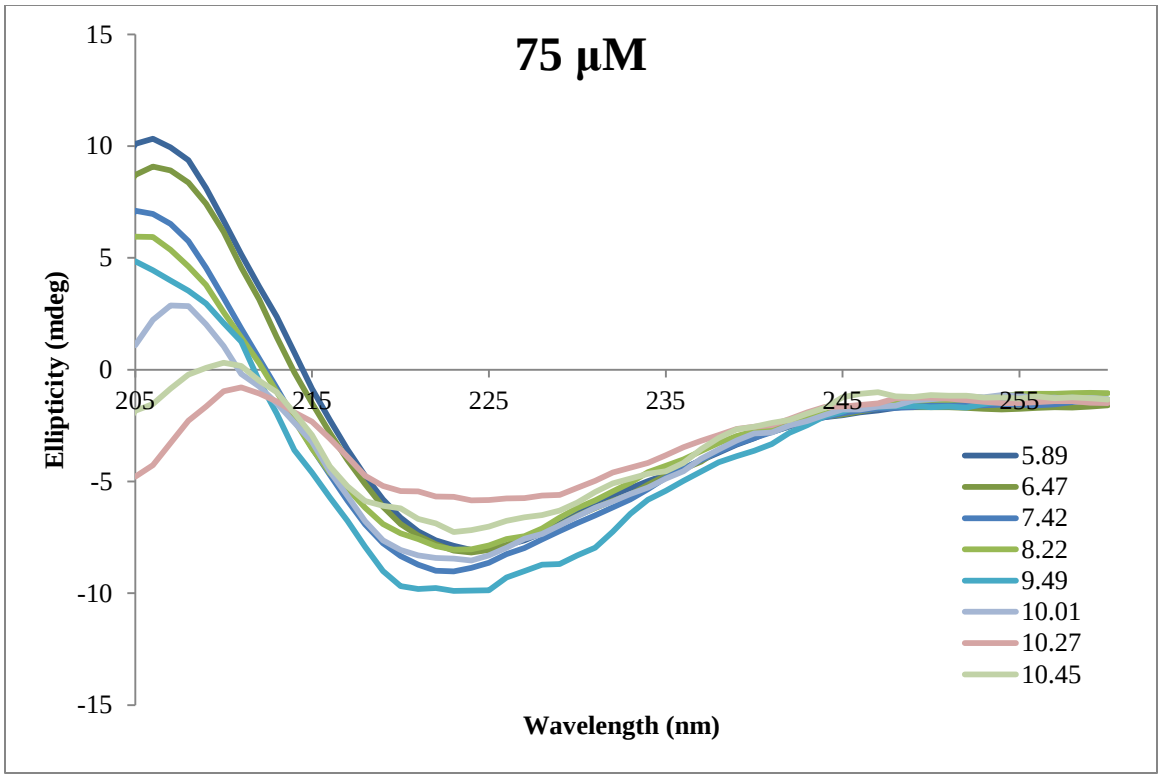
75 µM
Ellipticity (mdeg)
Wavelength (nm)
15
10
5
0
-5
-10
-15
205
215
225
235
245
255
5.89
6.47
7.42
8.22
9.49
10.01
10.27
10.45

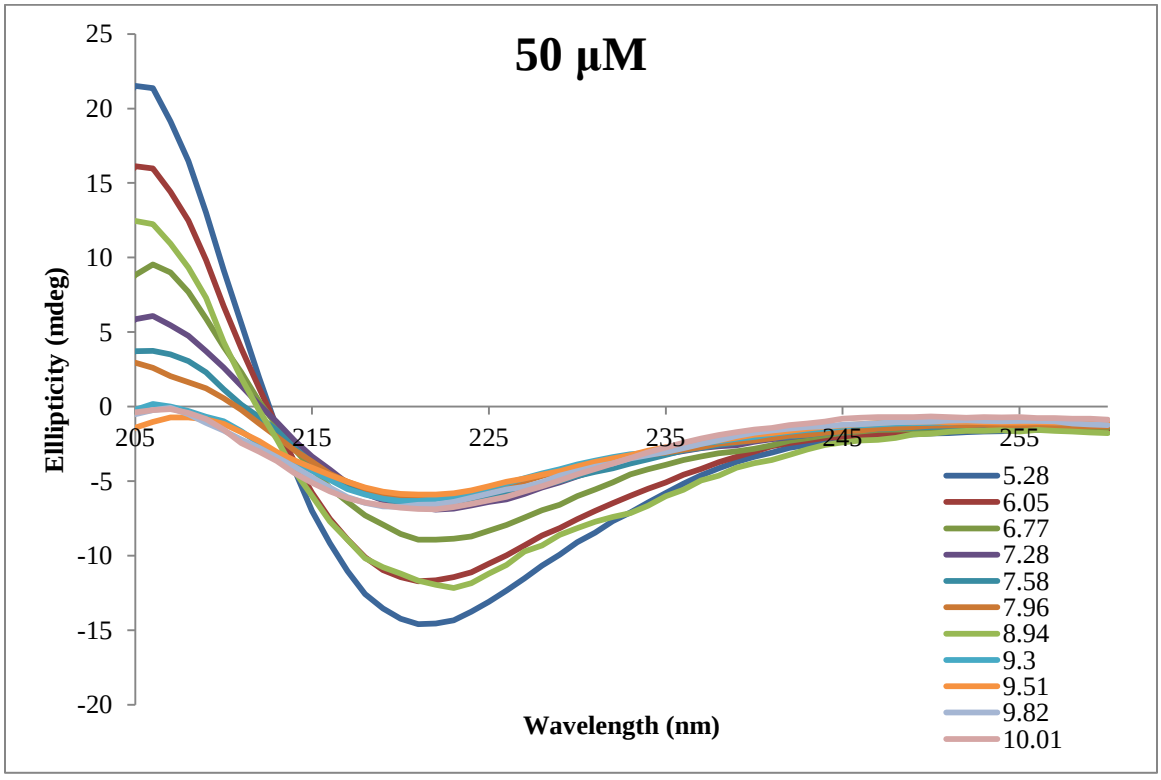
50 µM
Ellipticity (mdeg)
Wavelength (nm)
25
20
15
10
5
0
-5
-10
-15
-20
205
215
225
235
245
255
5.28
6.05
6.77
7.28
7.58
7.96
8.94
9.3
9.51
9.82
10.01

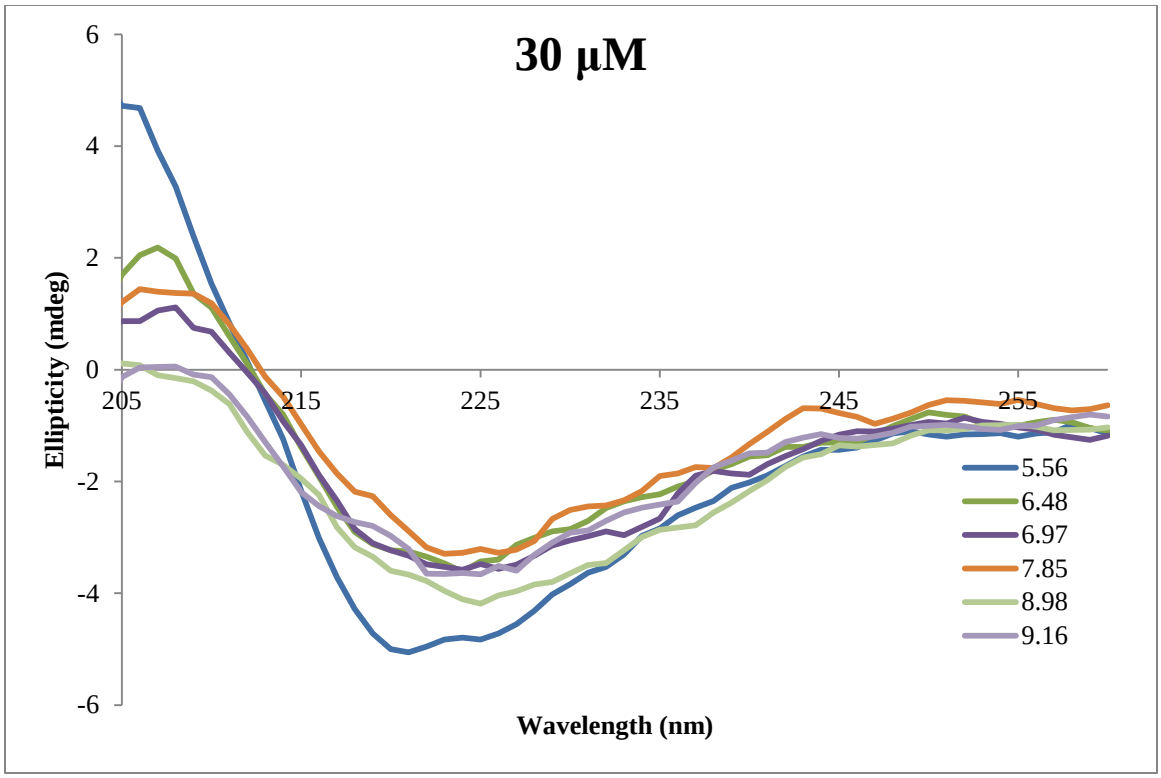
30 µM
Ellipticity (mdeg)
6
4
2
0
-2
-4
-6
205
215
225
235
245
255
Wavelength (nm)
5.56
6.48
6.97
7.85
8.98
9.16

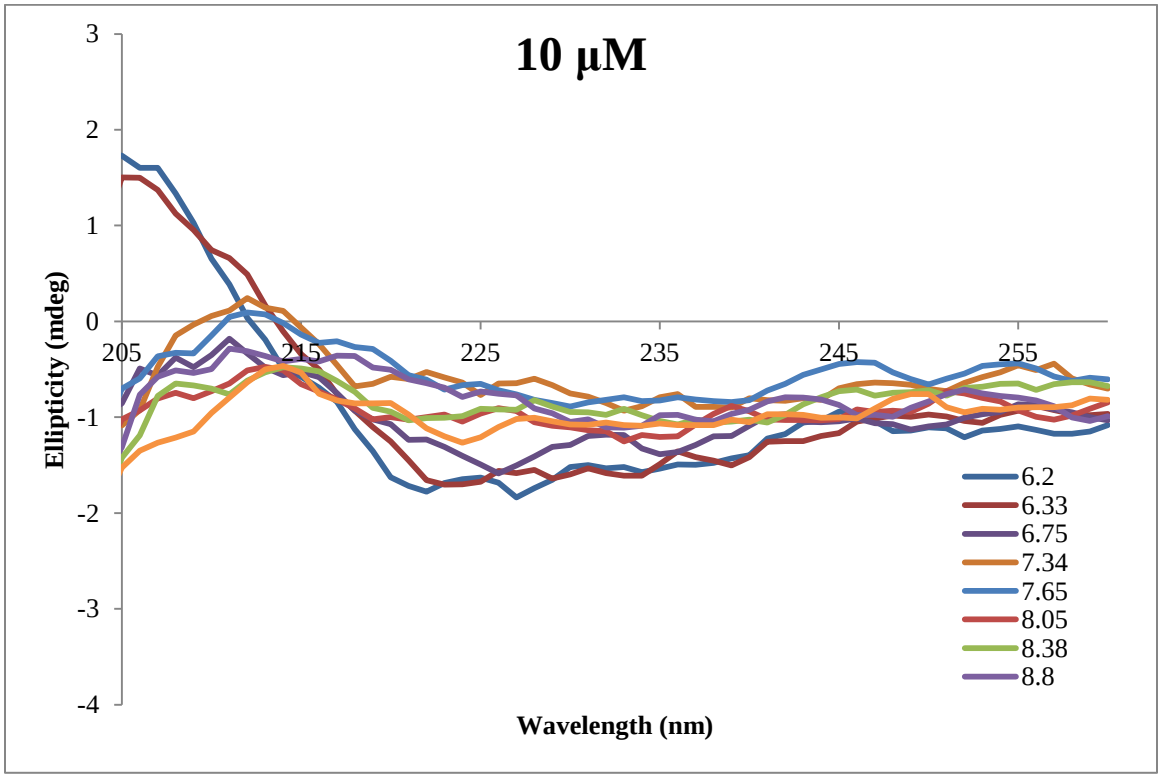
10 µM
Ellipticity (mdeg)
3
2
1
0
-1
-2
-3
-4
205
215
225
235
245
255
Wavelength (nm)
6.2
6.33
6.75
7.34
7.65
8.05
8.38
8.8

Circular Aggregation Concentration

CAC for PA 5 pH 5 in 150 mM NaCl and 2.2 mM $CaCl_2$

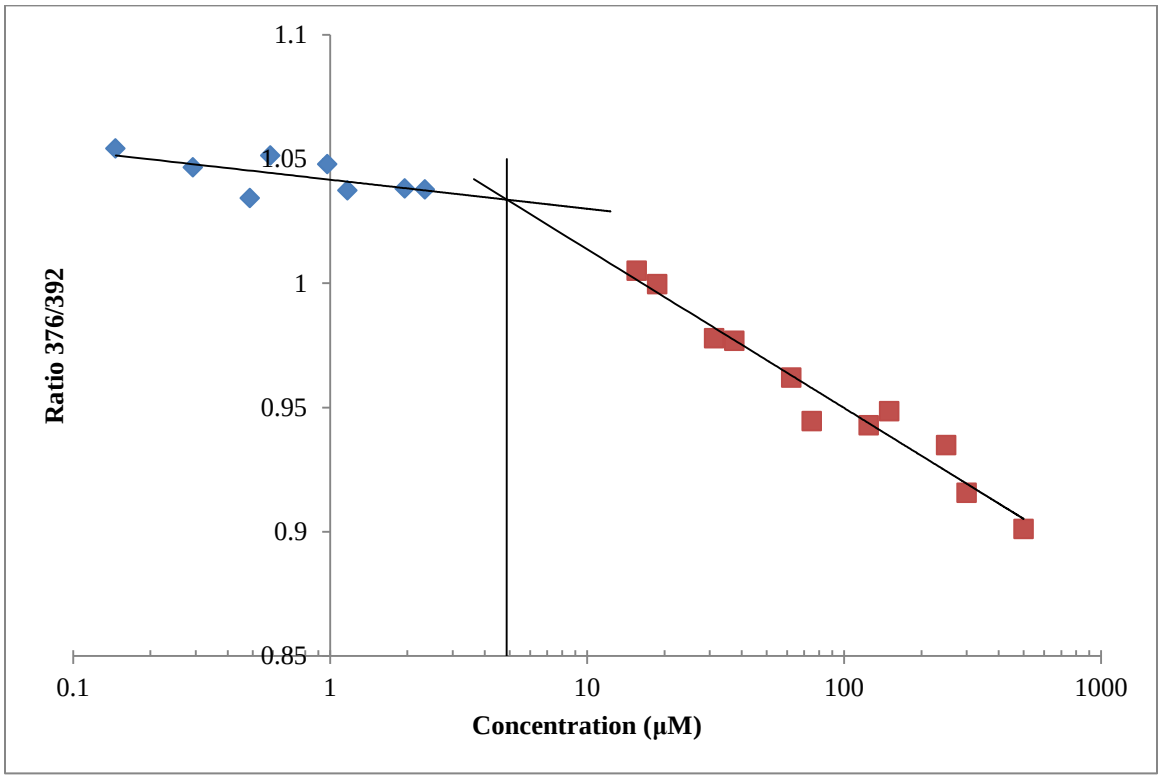

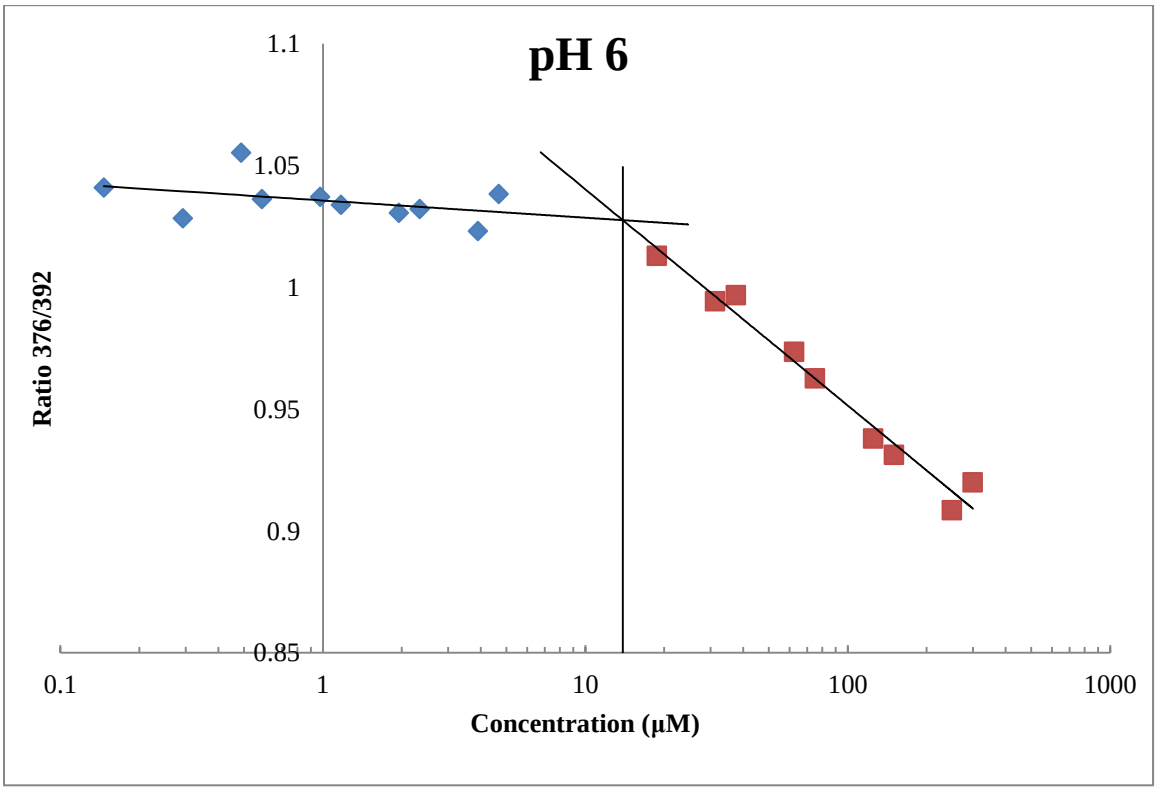

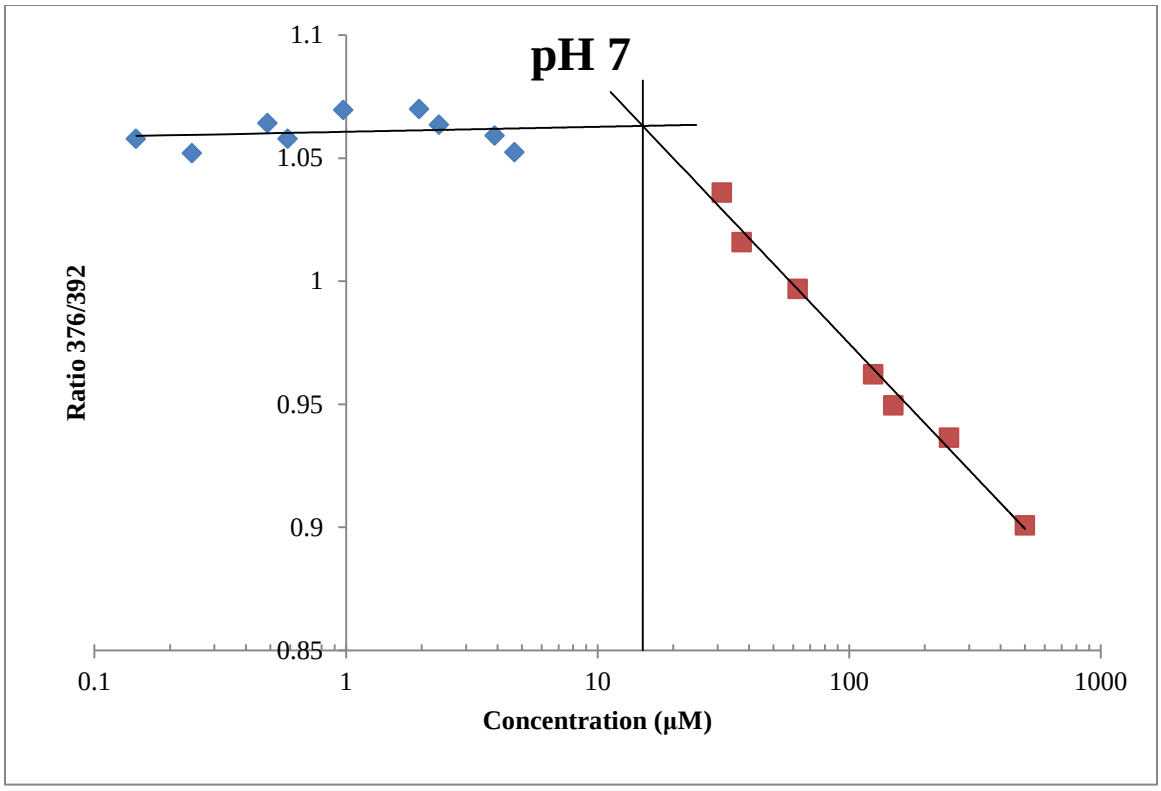
pH 7
Ratio 376/392
1.1
1.05
1
0.95
0.9
0.85
0.1
1
10
100
1000
Concentration (µM)

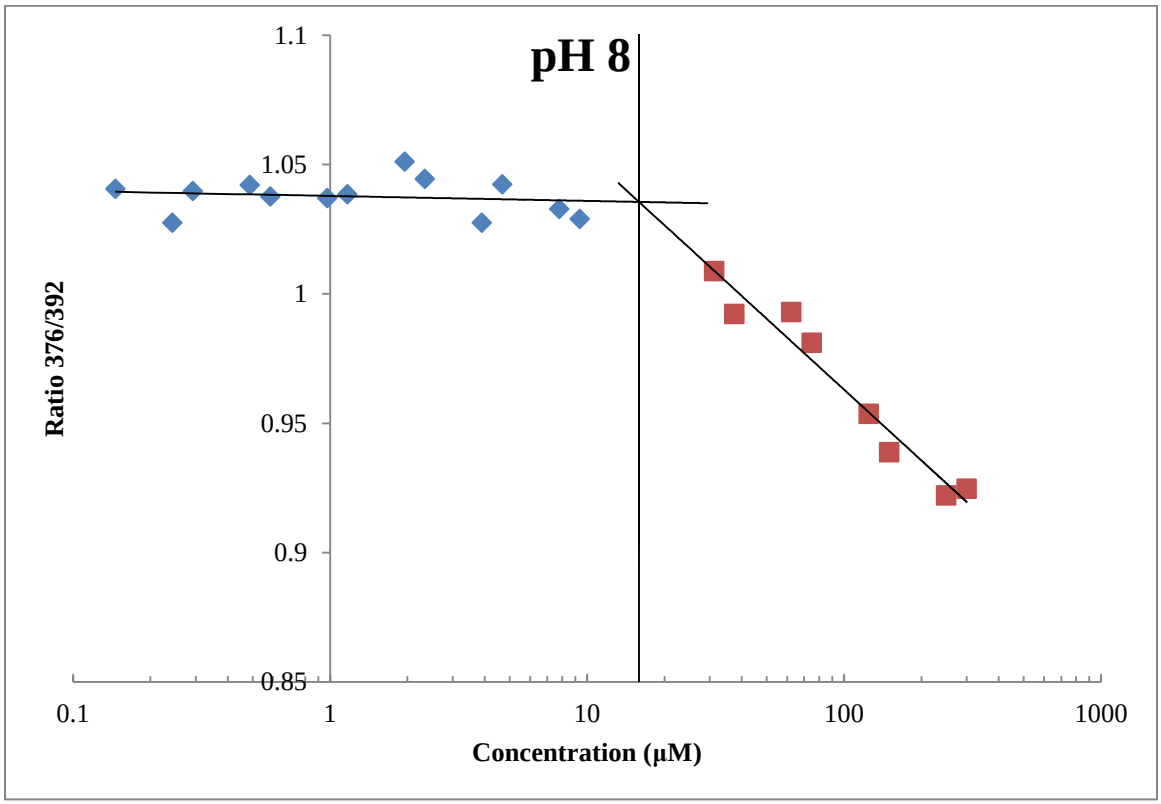
pH 8
Ratio 376/392
1.1
1.05
1
0.95
0.9
0.85
0.1
1
10
100
1000
Concentration (µM)

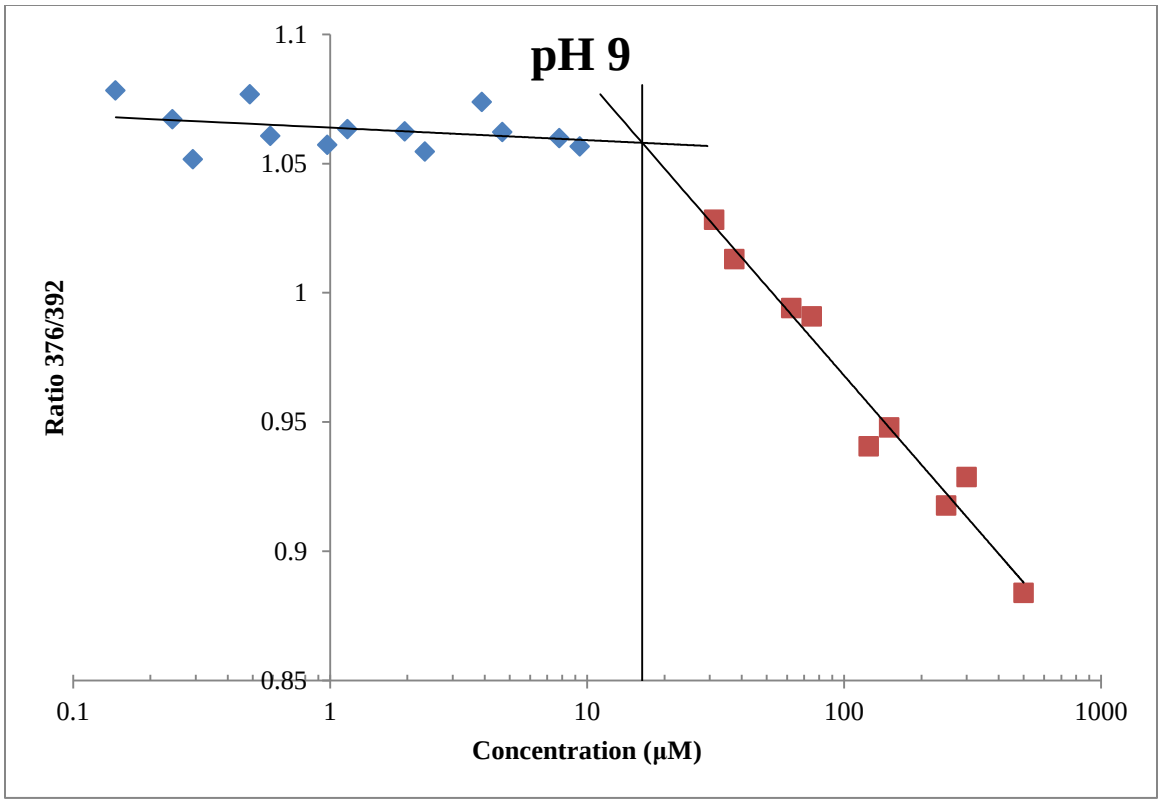

CAC for PA 6 in 150 mM NaCl and 2.2 mM $CaCl_2$

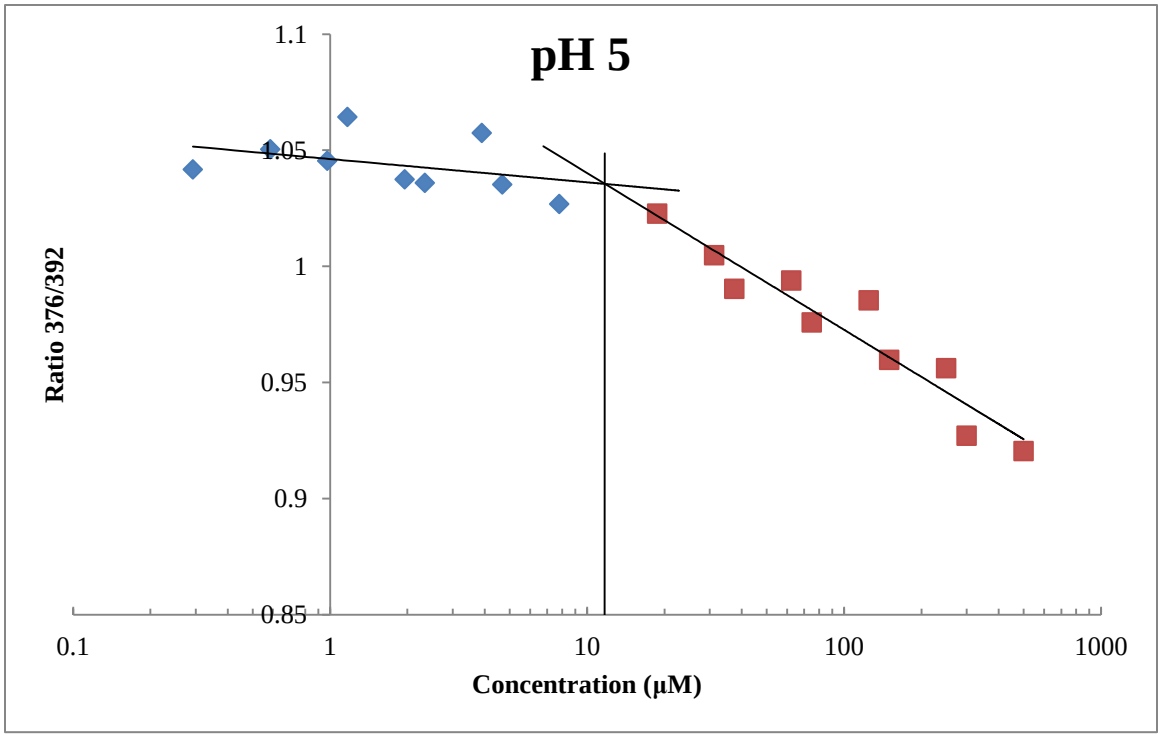

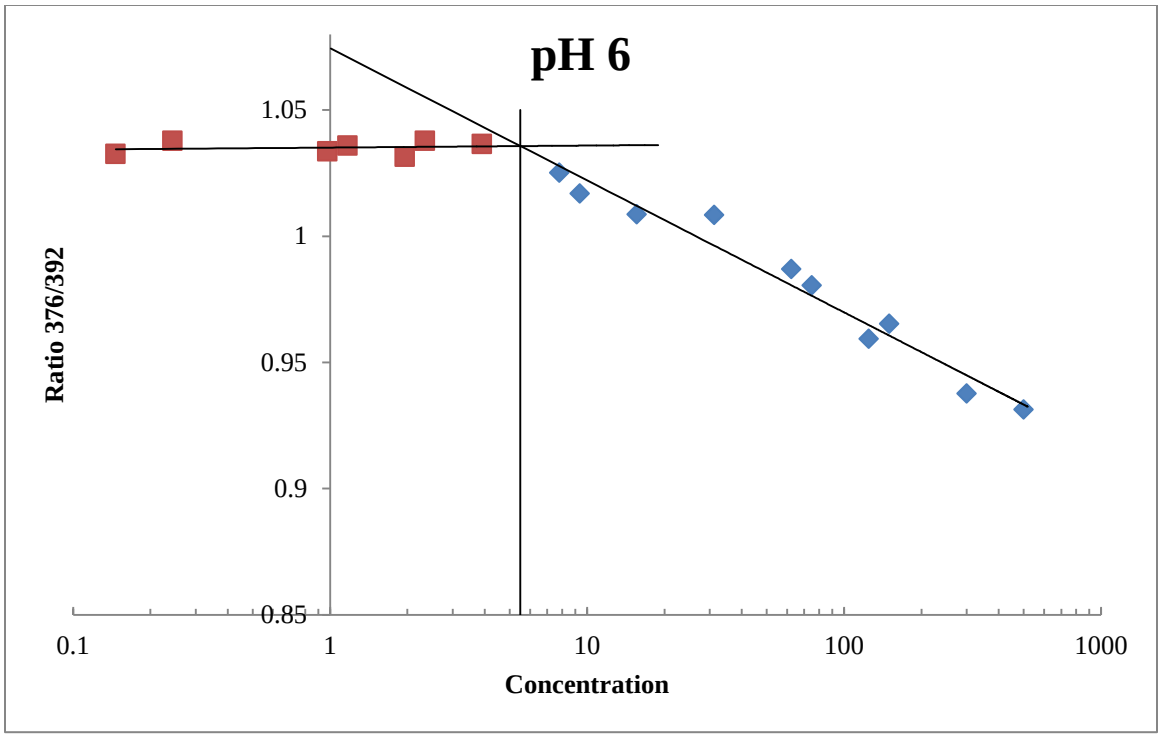
pH 6
1.05
1
0.95
0.9
0.85
Ratio 376/392
0.1
1
10
100
1000
Concentration

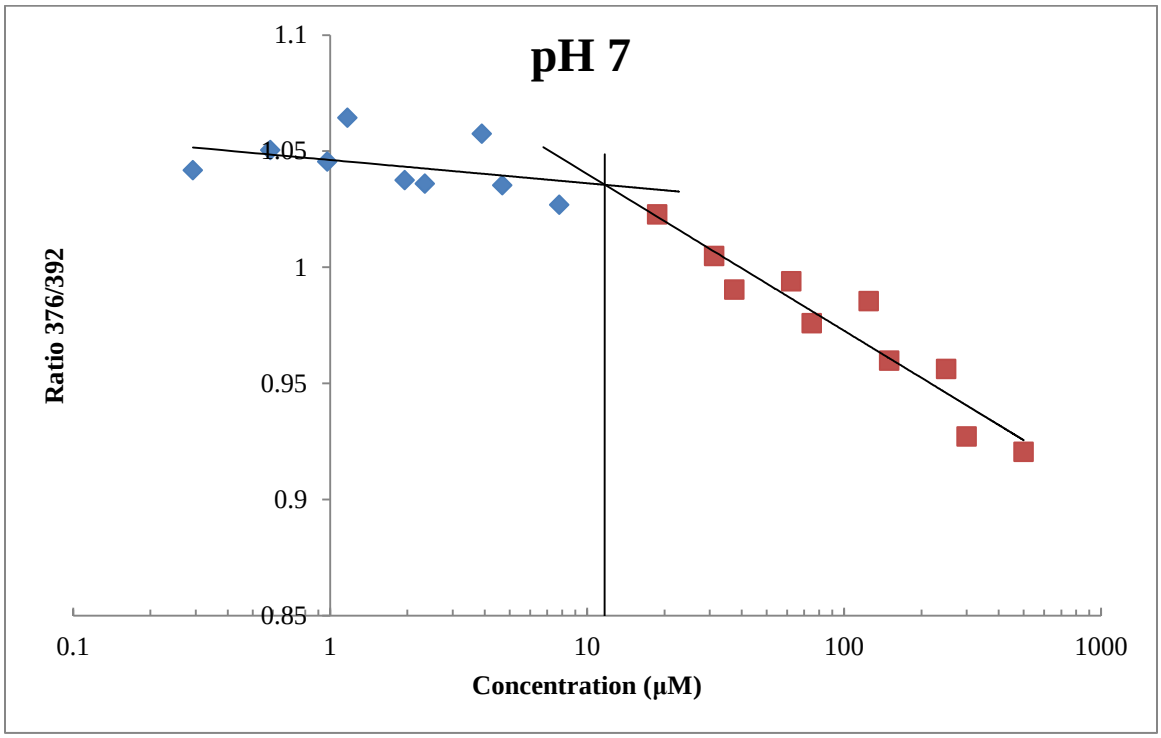
pH 7
1.1
1.05
1
0.95
0.9
0.85
Ratio 376/392
0.1
1
10
100
1000
Concentration (µM)

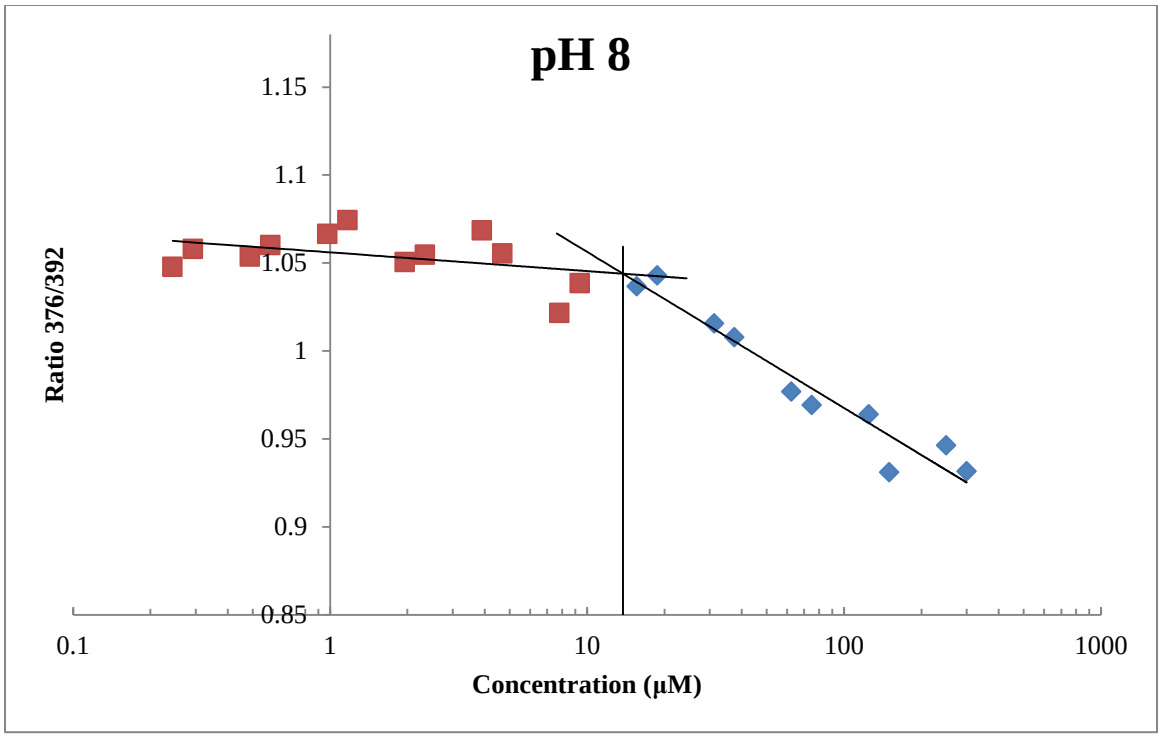
pH 8
1.15
1.1
1.05
1
0.95
0.9
0.85
Ratio 376/392
0.1
1
10
100
1000
Concentration (µM)

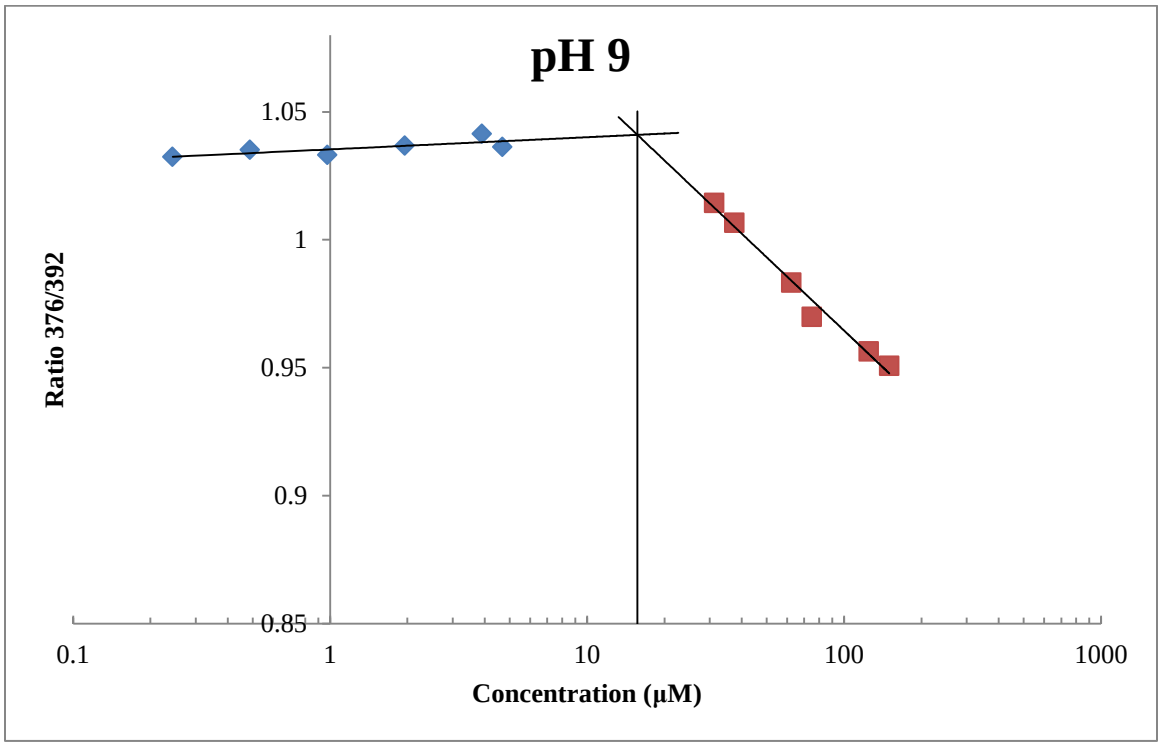
pH 9
1.05
1
0.95
0.9
0.85
Ratio 376/392
0.1
1
10
100
1000
Concentration (µM)

Table of CACs for PAs 2 – 6
(in μM)

pH	PA 2	PA 3	PA 4	PA 5	PA 6
5	0*	0*	7.28	*4.87*	5.50
6	5.62	1.18	11.31	*13.89*	11.72
7	9.37	3.89	14.08	*15.11*	13.79
8	12.58	12.04		*15.93*	14.71
9	21.59	25.47	15.45	*16.39*	15.69

*below the detectable limit

Dynamic Light Scattering
PA 2 – pH 10.2 50 μM in salt solution

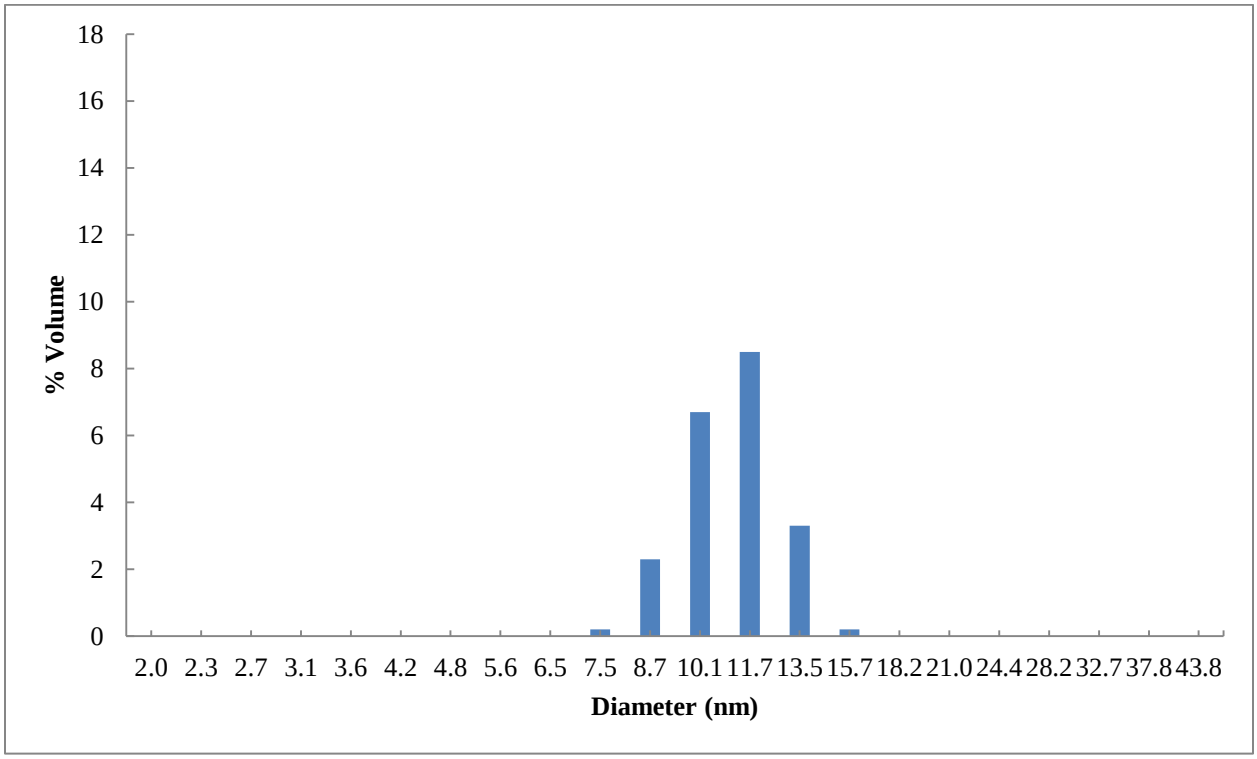

PA 3 – pH 10.5 50 µM in salt solution

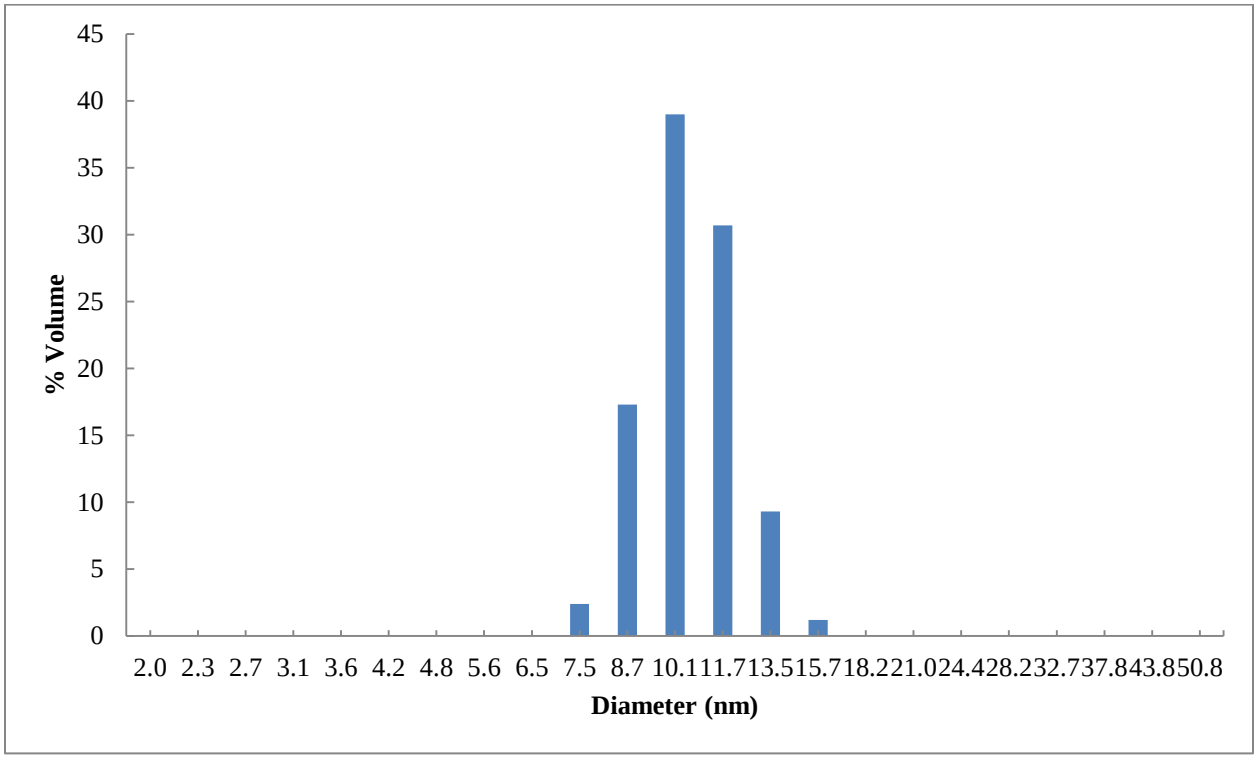

PA 4 – pH 10.6 50 µM in salt solution

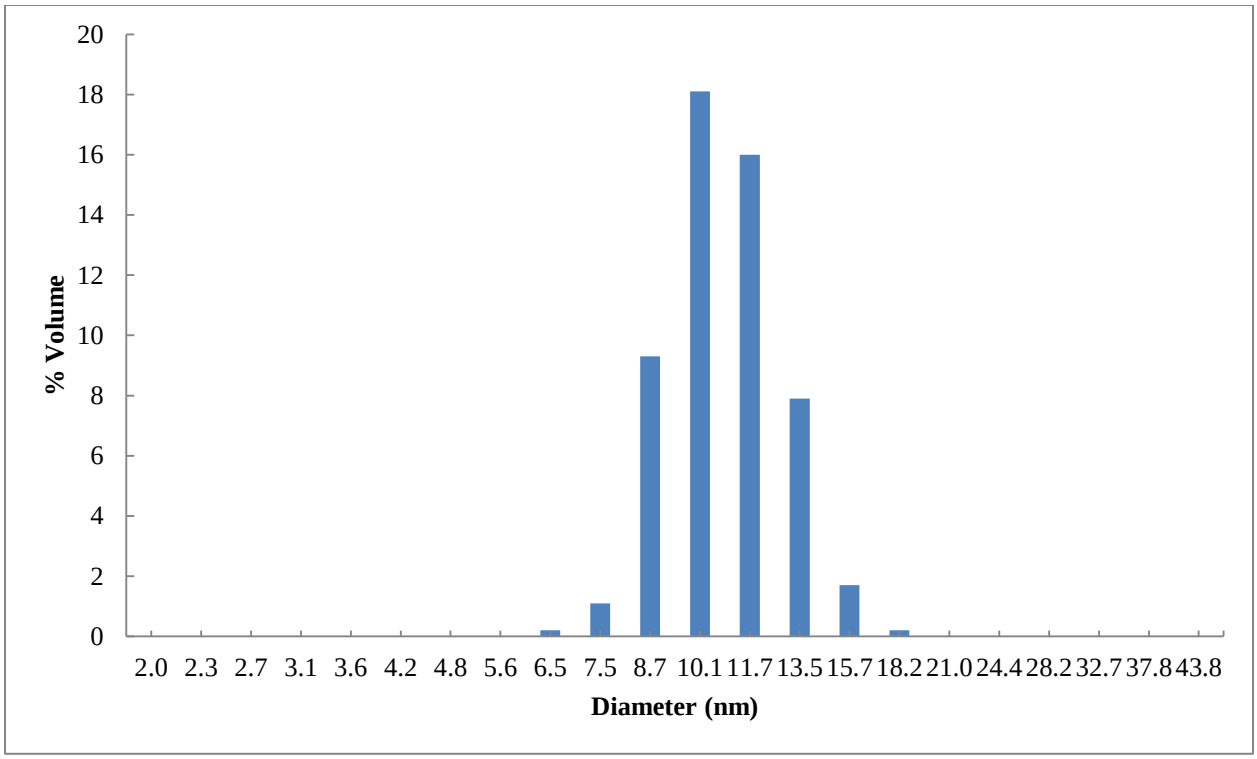

PA 5 – pH 10.5 50 µM in salt solution

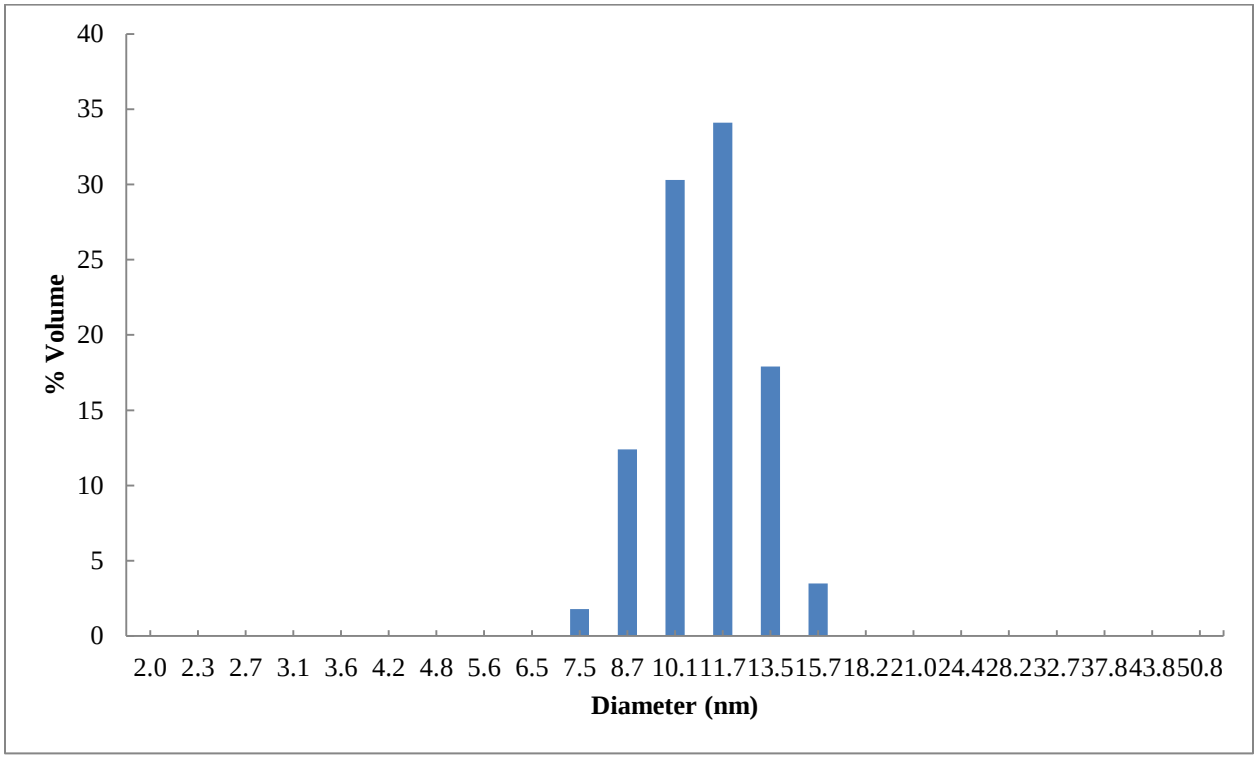

PA 6 – pH 10.8 40 µM in salt solution

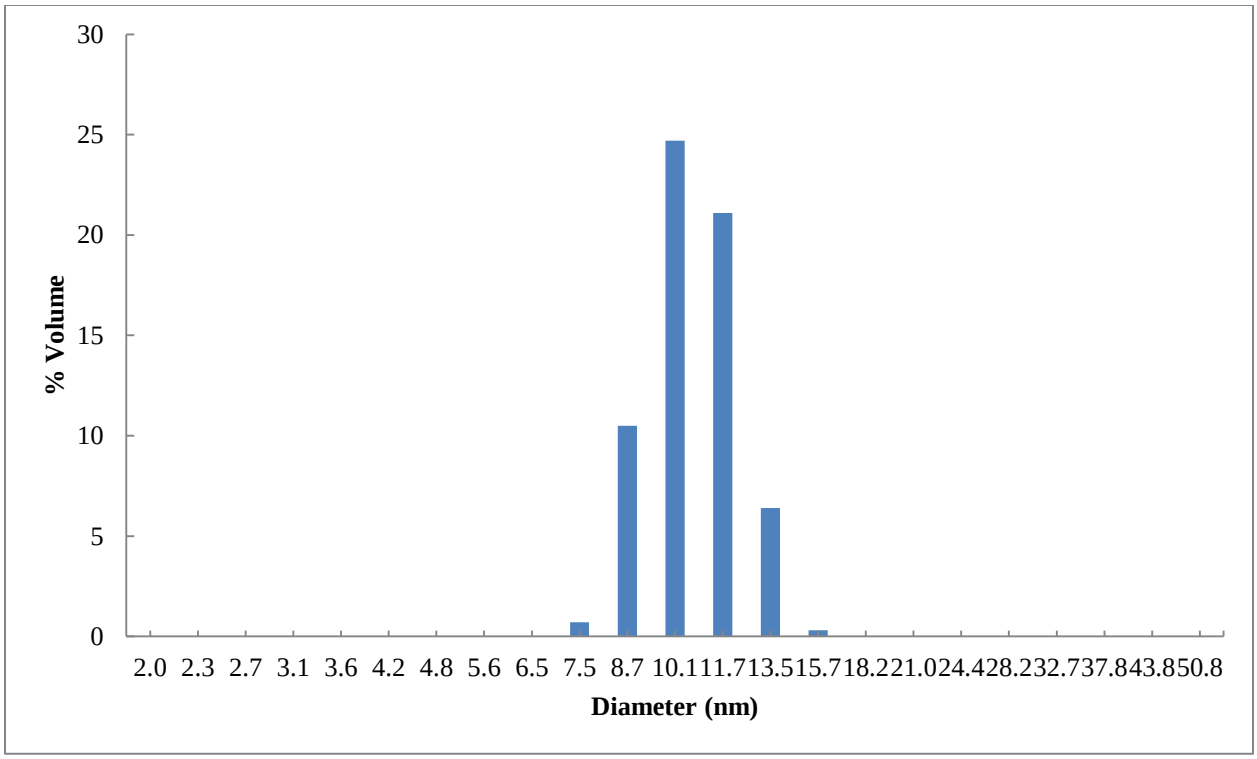

Chapter 8: Materials and Methods

Synthesis of Peptide Amphiphiles (PA):

All amino acids and coupling agents were purchased from AnaSpec INC. The peptides were synthesized via solid-phase Fmoc chemistry. The peptide sequence was built C-Terminus to N-Terminus using a Seiber Amide Resin (AAPPTEC) on a 0.3 mmol scale. All of the prepared PAs were synthesized manually as outlined in the following paragraph.

The resin was placed in a shaker vessel and then swollen with dichloromethane (DCM) for 30 minutes. The DCM was removed, and then N, N-Dimethylformanide (DMF) was added to the shaker vessel to swell the resin for 30 minutes. 20% piperidine in DMF was added for the deprotection of the Fmoc protecting group and allowed to shake for 15 minutes. The liquid was removed, and replenished to shake for another 15 minute interval. The piperidine/DMF solution was removed and washed with DCM, DMF (2x) and DCM (2x) sequentially. The removal of the Fmoc protecting group was confirmed via a Kaiser Test. The coupling solution for each amino acid contained 4 eq. of O-Benzotriazole N,N,N',N'-tetramethyluroniumhexafluorophosphate (HBTU) or 2-(7-Aza-1H-benzotriazole-1-ly)-1,1,3,3- tetramethyluronium hexafluorophosphate (HATU), 3.95 eq. of amino acid, 6 eq. of N,N- diisopropylethylamine (DIPEA) and 2 drops of Triton X-100 in approximately 10mL of DMF. This solution was added to the shaker vessel and allowed to couple for 3 hours to the deprotected species (amino acid or resin). The solution was then removed, and the resin was washed with DMF (3x) followed by DCM (2x). The coupling of the amino acid was confirmed by another Kaiser Test. This process was repeated for each amino acid as well as the palmitic or pentadecanoic acid tail.

Attachment of DO3A to PAs:

A solution containing 10% hydrazine in DMF was prepared and added to the resin in the shaker vessel to deprotect the 1-(4,4-dimethyl-2,6-dioxocyclohex-1-ylidene)-3-methylbutyl (ivDde) group from the side chain of the lysine. The vessel was shaken for 20min, the solution drained, and this process was repeated twice more for a total of three washes. A coupling solution containing 2 eq. HATU, 2 eq. 1,4,7- tris(carboxymethylaza)cyclododecane-10-azaacetylamide (DO3A), 4.4 eq. DIPEA (relative to the PA) were added to the shaker vessel. The mixture was then set to stir for 18-24 hours at room temperature. To ensure maximal coupling, excess solvent was removed under vacuum, until only 10-15 mL of the mixture remained. A second coupling mixture of 2 eq. HATU, 4.4 eq. DIPEA and 1 mL of pyridine was added to the PA and stirred for 18-24 hours.

Resin Cleavage and removal of tert-butyl groups on PA:

A 20 mL solution containing 95% TFA, 3% water and 2% Anisole was prepared and added to the PA-DO3A. The mixture was set to stir for 20-24 hours at room temperature in order to remove tert-butyl groups from the glutamic acid, tyrosine and DO3A species. Excess TFA was removed under vacuum and the PA-DO3A was crashed out with cold diethyl ether. The mixture was cooled at -5°C for 45 minutes and the resulting solid was isolated via filtration.

Purification of PA-DO3A:

The crude PA-DO3A (150-250 mg) was dissolved in a 10 mL solution consisting of 9 mL of water, 1 mL of acetonitrile and a few drops of NH_4OH. This solution was, shaken, sonicated and vortexed to ensure full dissociation. The resulting solution was then filtered

through a 0.45 µm PVDF filter. Purification of the PA-DO3A was carried out using a Shimadzu preparative High Performance Liquid Chromatograph (HPLC) duel pump system controlled by LC-MS solution software, with an Agilent PLRP-S polymer column (Model No. PL1212.3100 150 mm x 25 mm). The two solvents that were used for the mobile phase were water with 0.1% NH_4OH (v/v) and acetonitrile with 0.1%NH_4OH (v/v). The product was eluted via a linear gradient from 10% acetonitrile to 20% acetonitrile over 22.5 minutes, and then from 20% acetonitrile to 40% acetonitrile over an additional 67.5 minutes. The desired product was collected in fractions of 10-15 mL. The presence of the product in the fractions was confirmed by a Bruker Electrospray Ionization Time of Flight Mass Spectrometry (ESI-TOF MS) and the purity by Shimadzu analytical HPLC. Fractions ≥ 95% in purity were added together, acetonitrile was removed under vacuum and the liquid fraction were freeze-dried yield a white powder.

Incorporation of Gd^{3+} in PA-DO3A:

The pure PA-DO3A was dissolved in 4-6 mL of water. 2 eq. of 0.01M $GdCl_3$ in 0.01M HCl were added to the PA-DO3A solution. Diluted NaOH(aq) was added to this solution to set the pH at 5.0 - 5.1. The solution was placed in an oil bath to stir at 60°C. After 60 minutes, the solution was removed from the oil bath, the pH was readjusted to a value of 5.0 – 5.1, and then placed back in the hot oil bath to stir for 12-18 hours. The solution was then returned to room temperature and the pH was raised to a value greater than 10 using 1 M NaOH to precipitate out all non-chelated Gd^{3+} to produce solid $Gd(OH)_3$. The solution was filtered with a 0.45 µm PVDF filter and the pH was lowered to a neutral value of approximately 7.

Dialysis of the PA-(DO3A:Gd):

The PA-(DO3A:Gd) solution was pipetted into a Spectra/Por® Biotech Cellulose Ester dialysis membrane (molecular weight cut off: 500 g/mol) and placed in 4 L of Millipore water. The water was changed 5 – 8 times over a 72 hour period. The dialyzed solution was then lyophilized. The resulting solid yielded the pure PA-(DO3A:Gd) powder which was confirmed through ESI- TOF MS and analytical HPLC.

Circular Dichorism (CD):

The PA-(DO3A:Gd) solid was dissolved in a aqueous solution of 150 mM NaCl and 2.2 mM CaCl2, to yield a 0.5 – 1 mM peptide solution. The resulting solution was then used to create diluted samples that included 500, 300, 100, 50, 30 and 10 μM. The pH was raised in each of the solutions to a value greater than 9, stirred in an oil bath at 90 °C for 30 minutes, and then cooled to room temperature. CD measurements were conducted on a JASCO J-815 Spectrometer using a 0.5 or 1 cm path length quartz cuvette. Three accumulation were measured at a wavelength range of 260 – 190 nm at a scanning speed of 100 nm/min with an integration time of 2 or 4 seconds for each data series. A baseline (aqueous salt solution) was subtracted from each of the measurements. Each molecule in this study was analyzed with these parameters at a range of concentration and pH values.

Critical Aggregation Concentration (CAC):

CAC for the synthesized molecules were determined using the pyrene 1:3 method[23]. CAC measurements were taken at pH points of 5, 6, 7, 8, and 9 for each of the molecules tested. 5 mg of pyrene were dissolved and mixed in methanol overnight and then diluted with NaCl, $CaCl_2$

aqueous solutions, and excess water to yield a solution of 150 mM NaCl, 2.2 mM $CaCl_2$ and 62 μM pyrene.

For the 500 μM PA-(DO3A:Gd) solution, the pH was raised to a value greater than 9, stirred in an oil bath at 90 °C for 30 minutes, and then cooled to room temperature. A 300 μM sample was made from this solution. 250 μL of both the 500 μM and 300 μM solutions were serial diluted with 150 mM NaCl 2.2 $CaCl_2$ mM aqueous solution. Each of the starting concentrations and the diluted mixtures were added to a 96-microwell plate. 5 μL of the pyrene solution was added to each of the wells and then stirred ensure homogeneity. All of the components added to make the samples were at the same pH value in order to test the CAC. The fluorescence emission of the pyrene was monitored by a BioTek Synergy H4 fluorimeter at an excitation wavelength of 335 nm. The pyrene fluorescence was monitored from 360 nm to 430 nm, and the peaks of maximum fluorescence intensity (usually at 376 nm and 392 nm were compared at different concentration values to determine the CAC at a specific pH value.

Dynamic Light Scattering (DLS):

PA was dissolved in 150 mM NaCl, 2.2 mM $CaCl_2$ and filtered with 250nm filters, and sonicated. The resulting solutions were adjusted to appropriate concentrations and pHs such that they exhibited a micelle morphology (typically 50 μM and pH = 10.5). DLS measurements were performed using a Malvern Nano series Zetasizer.

T_1 Relaxivity (r_1):

Various concentrations of PA-DO3A:Gd in 150 mM NaCl and 2.2 mM $CaCl_2$ were prepared to acquire low-field spin−lattice (T_1) relaxation time measurements at different pH

values on a benchtop minispec mq20. A permanent magnet created a field (0.469 T) corresponding to a proton resonance frequency of 19.95 MHz. The sample temperature was kept at 40 °C. For all samples, the magnetic field was matched to the resonance circuit, and the durations were on the order of 2.8 and 5.6 μs at full amplitude for π/2- and π-pulses, respectively. The inversion−recovery pulse sequence was used to measure the 1 H T_1 relaxation times in the laboratory frame. In this pulse sequence, the bulk magnetization is inverted by a 180° radio frequency pulse and then allowed to recover to equilibrium via the T_1 relaxation process over a variable recovery time, before acquisition of the free-induction decay with 32 data points and 16 scans per point. A recycle delay time of >5 T_1 was used to allow the system to fully relax between FID acquisitions, and phase cycling was employed to eliminate signal artifacts. Relaxivity (r_1) values were then obtained from the slopes of $1/T_1$ vs PA:Gd(DO3A) plots.

References

(1) "Cancer Facts & Figures 2016" American Cancer Society. Web. **2016**

(2) "Estimates of Funding for Various Research, Condition, and Disease Categories" National Institute of Health. Web. **2016**

(3) Dhanasekaran, S.M., et al; *Nature*, **2001**, 412,822-6

(4) Palerba, D., et al, *New England Journal of Medicine*, **2016**, 374, 211-222

(5) "Biomarkers In Risk Assessment: Validity And Validation" World Health Organization. Web. **2001**

(6) Gatenby, R., et al. *Nature Reviews Cancer*, 2004, 4 (11), 891-9

(7) McDonald, D. M., and Baluk, P. *Cancer Research*, **2002**, 62; 5381

(8) Ghosh, A. et al; *JACS*, **2012**, 134 (8), 3647-50

(9) Chauhan, V.P., et al; *Nature Nanotechnology*, **2012**, 7, 383-8

(10) Preslar, A.T., et al; *ACS Nano*, **2014**, 8 (7), 7325-32 (11) Amblard, M., et al; *Molecular Biotechnology*, **2006**, 33(3), 239-54

(12) Nicholl, Michael J. Thesis. The Ohio State University, **2014**.

(13) Kim, C.A., et al; *Nature Letters*, **1993**, 362, 267-70

(14) Ghosh, A., et al; *JACS*, **2014**. 15 4488-4494

(15) Aguiar, J., et al; *Journal of Colloid and Interface Science*, **2003**, 258, 116-22

(16) *CRC Handbook of Chemistry and Physics*, 89th ed.; Lide, D.R., Ed.; CRC Press: Boca Raton, FL, 2008; Section 5.

(17) Schmid. *Encyclopedia of Life Sciences*. **2001**

(18) Perazella. *CJASN*, **2009**, 4, 461-469